Citation for published version:
Chew, J 2004, 'CFD Studies of Dynamic Gauging', *Chemical Engineering Science*, vol. 59, no. 16, pp. 3381-3398. https://doi.org/10.1016/j.ces.2004.03.042

DOI:
10.1016/j.ces.2004.03.042

Publication date:
2004

Link to publication

University of Bath

Alternative formats
If you require this document in an alternative format, please contact:
openaccess@bath.ac.uk

General rights
Copyright and moral rights for the publications made accessible in the public portal are retained by the authors and/or other copyright owners and it is a condition of accessing publications that users recognise and abide by the legal requirements associated with these rights.

Take down policy
If you believe that this document breaches copyright please contact us providing details, and we will remove access to the work immediately and investigate your claim.

Download date: 05. May. 2023

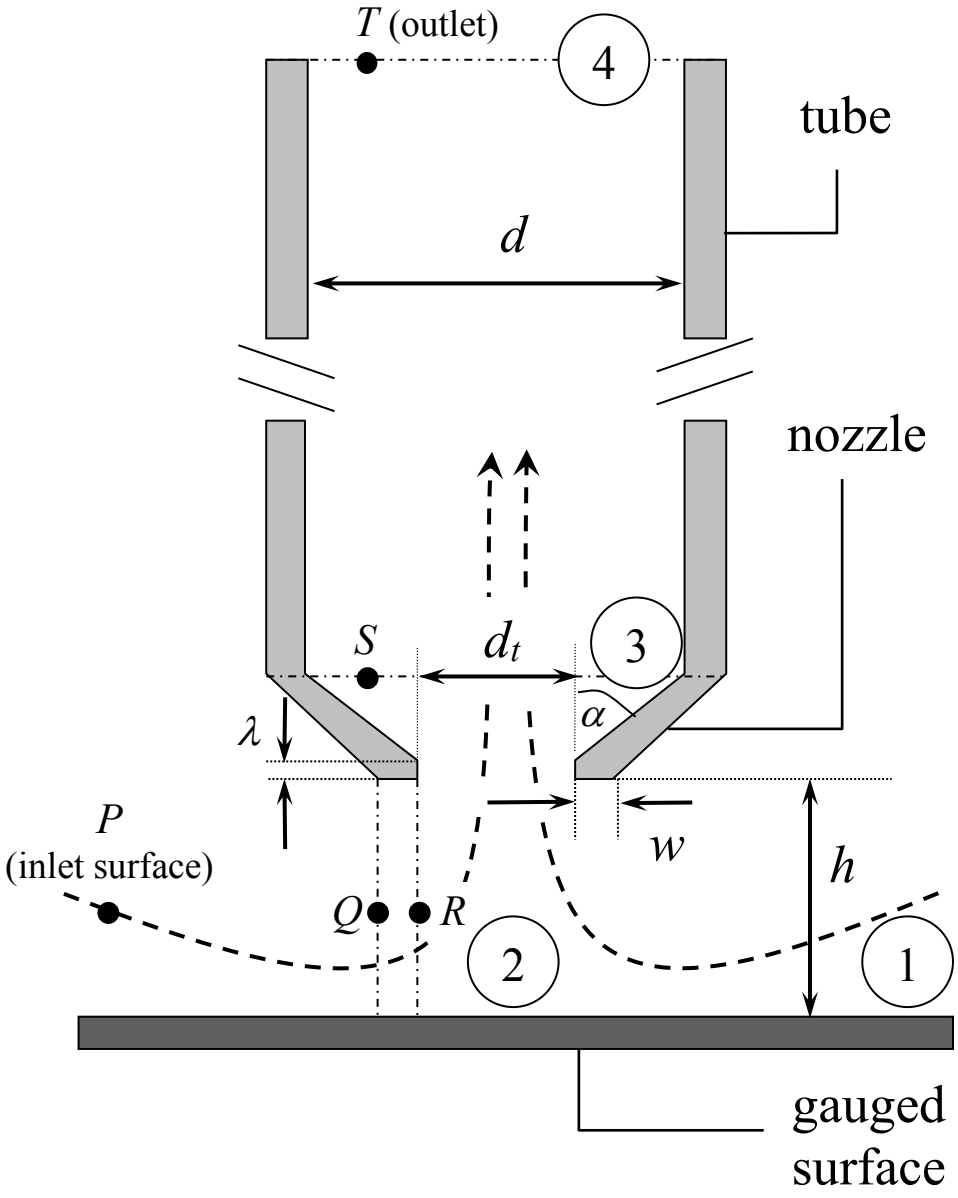

Figure 1: Schematic of a typical gauging nozzle showing dimensions.
a) **1** – **4** are flow stations.
b) *P* – *T* are points showing the different sections for pressure drop analysis (*PQ* – convergent section, *QR* – area under the rim, *RS* – divergent section, *ST* – tube section).

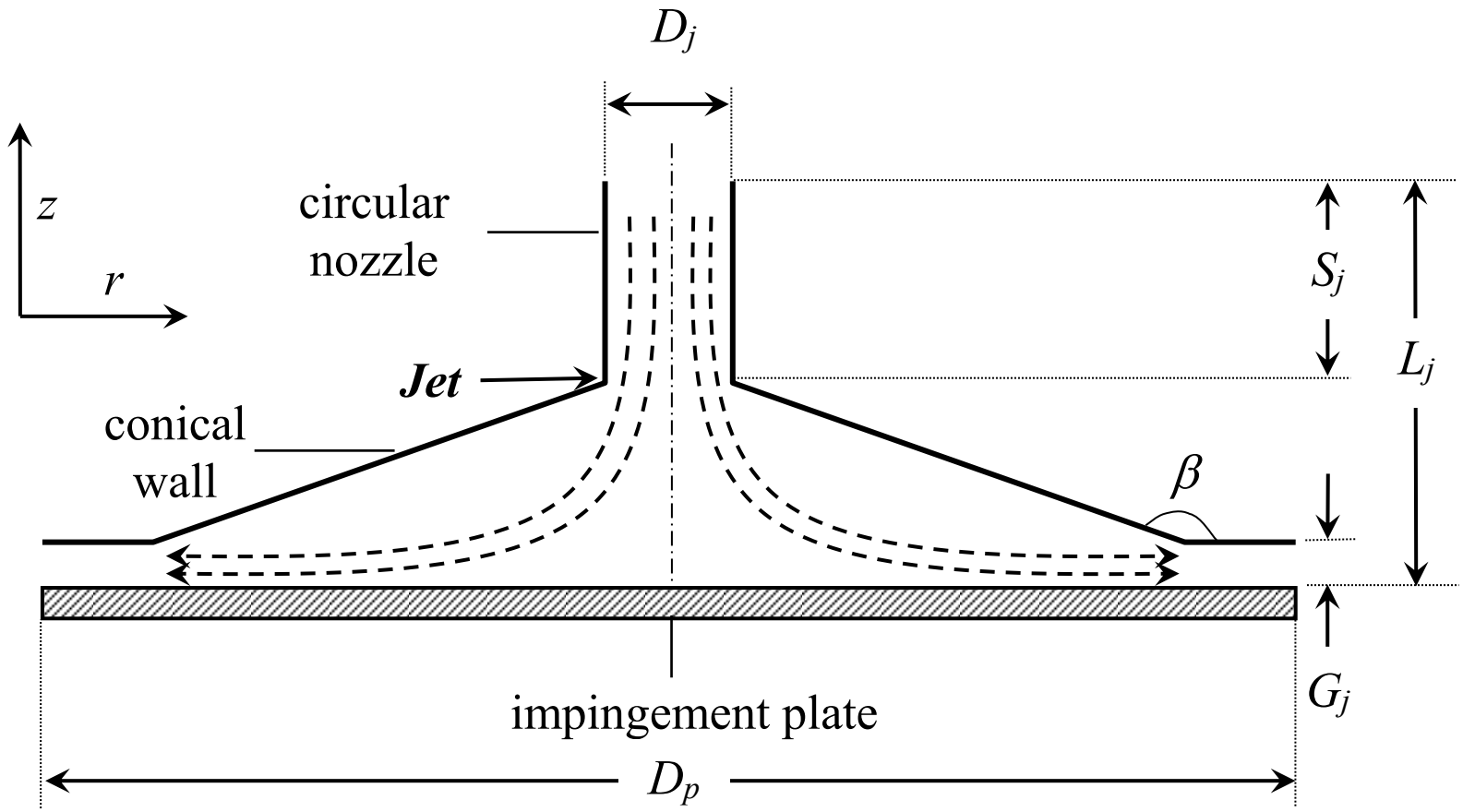

Figure 2: Schematic of a conical cell showing the ratios of dimensions.
($D_p/D_j = 8$, $L_j/D_j = 1$, $S_j/D_j = 0.35$, $G_j/D_j = 0.1$, $\beta = 168.9^o$)

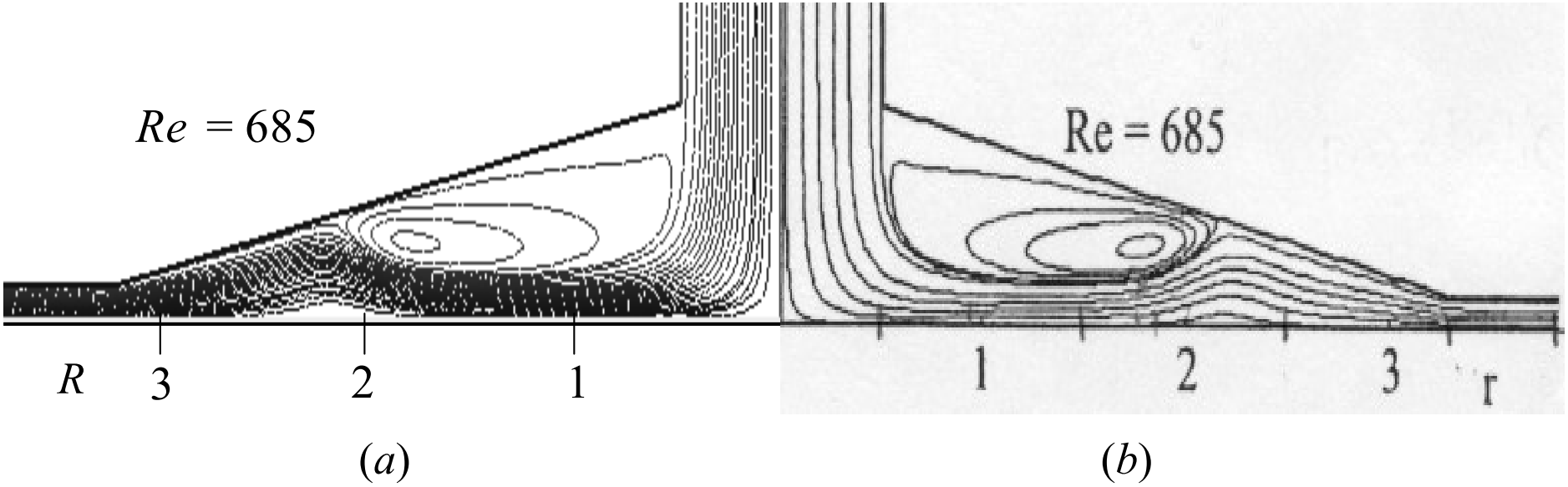

Figure 3: Comparison of predicted streamlines at Re = 685.
(a) – this work, (b) – Miranda & Campos (1999).

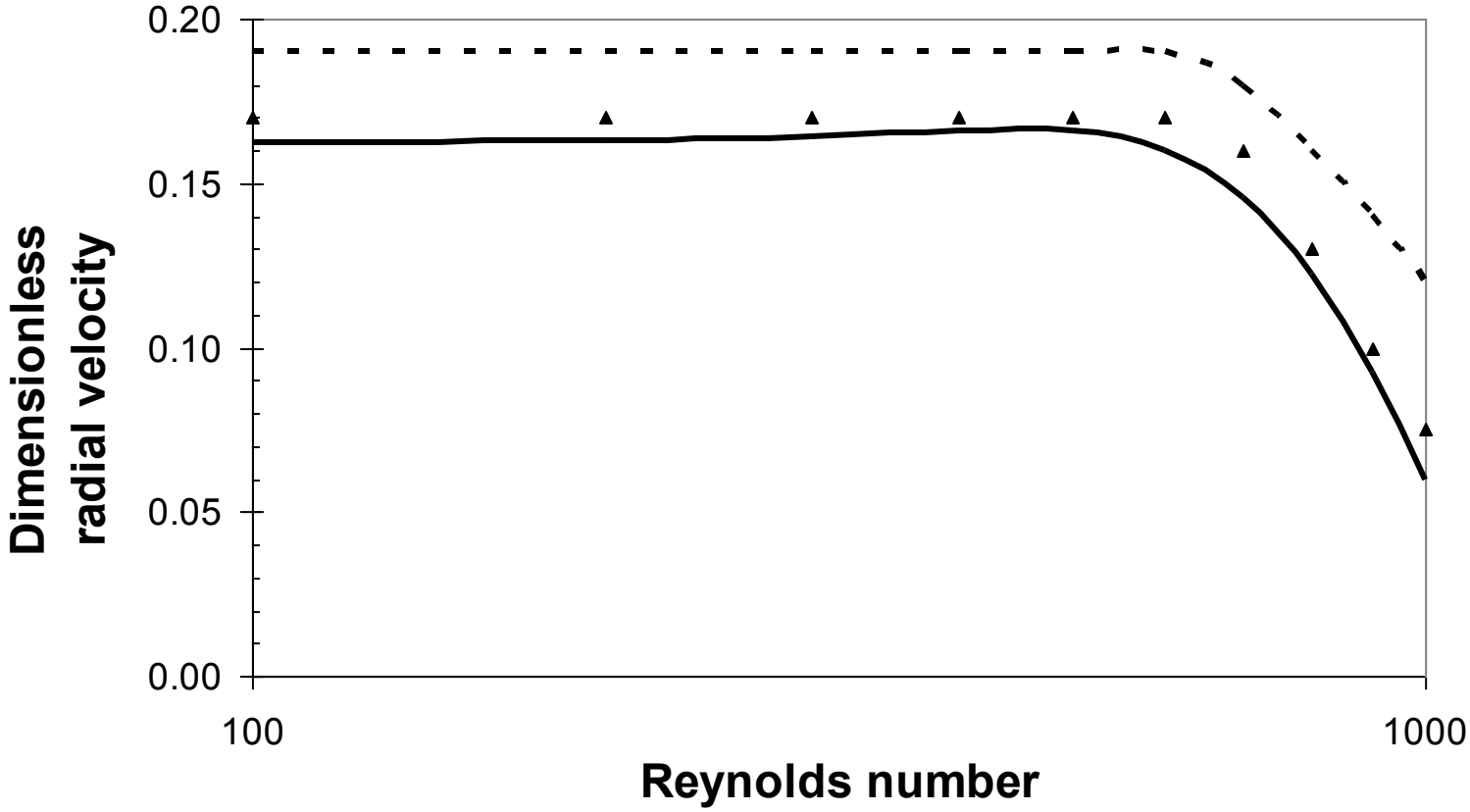

Figure 4: Comparison of radial velocities at one point within the conical cell, $R = 2.65$, $Z = 0.034$.
Solid line – this work; squares – experimental data (Miranda & Campos, 1999); dotted line – numerical predictions (finite difference, Miranda & Campos, 1999).

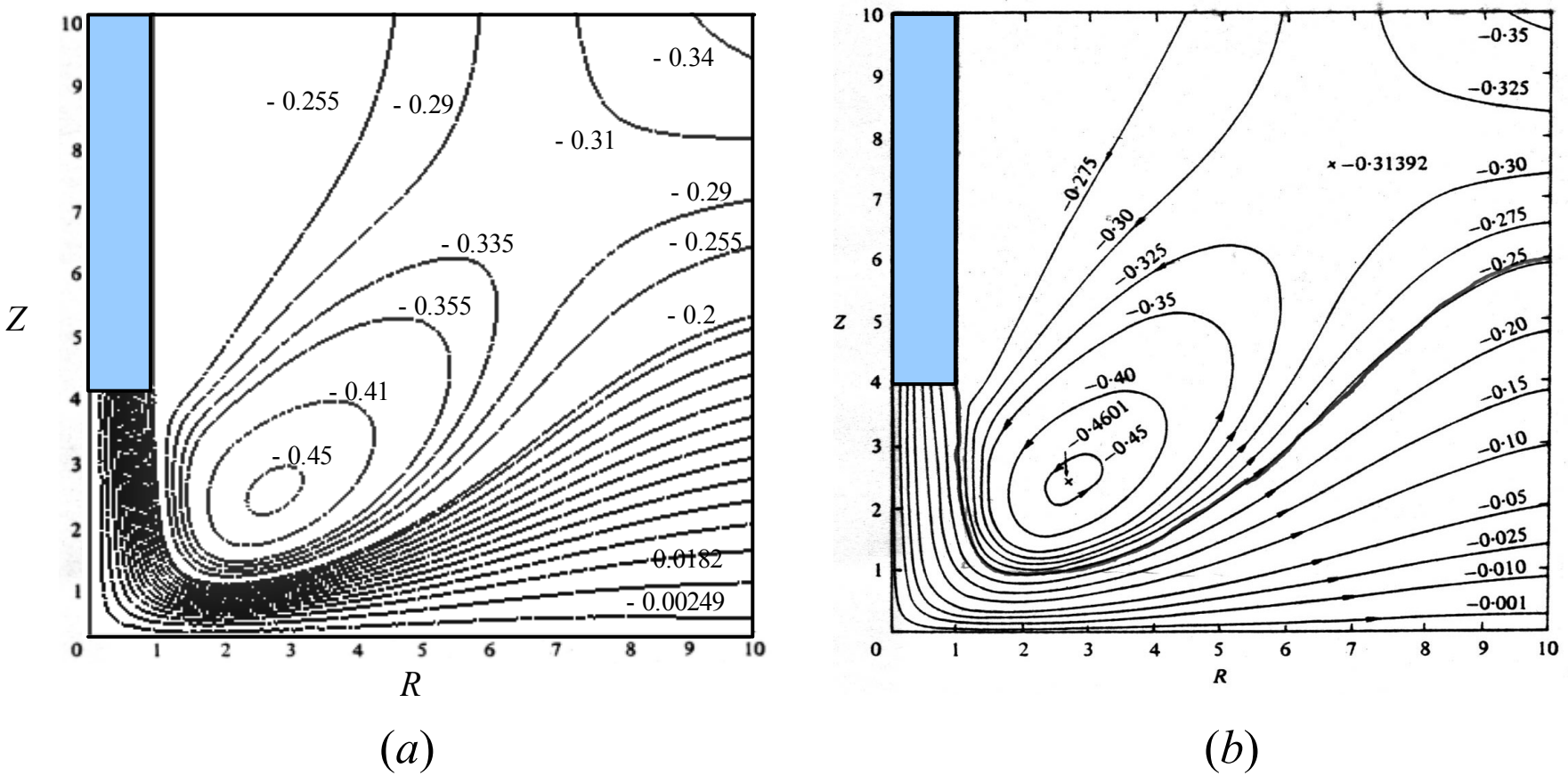

Figure 5: Comparison of streamline predictions for impinging laminar submerged jet at $Re = 25$, defined at the jet exit. (*a*) – this work, (*b*) – Deshpande & Vaishnav (1982).

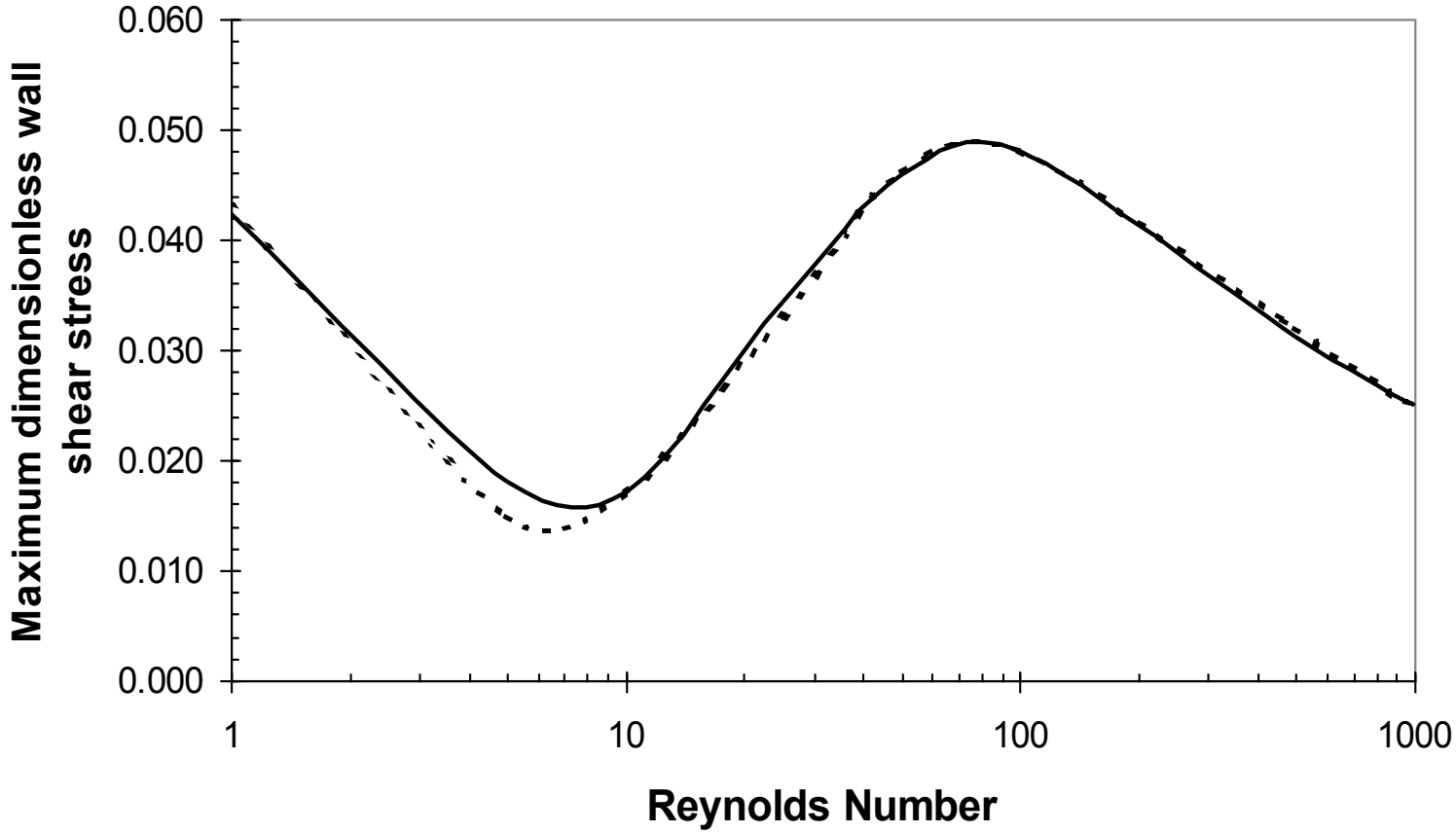

Figure 6: Comparison of predictions of the maximum dimensionless wall shear stress for an impinging laminar jet. Solid line – this work; dotted line –Deshpande & Vaishnav (1982).

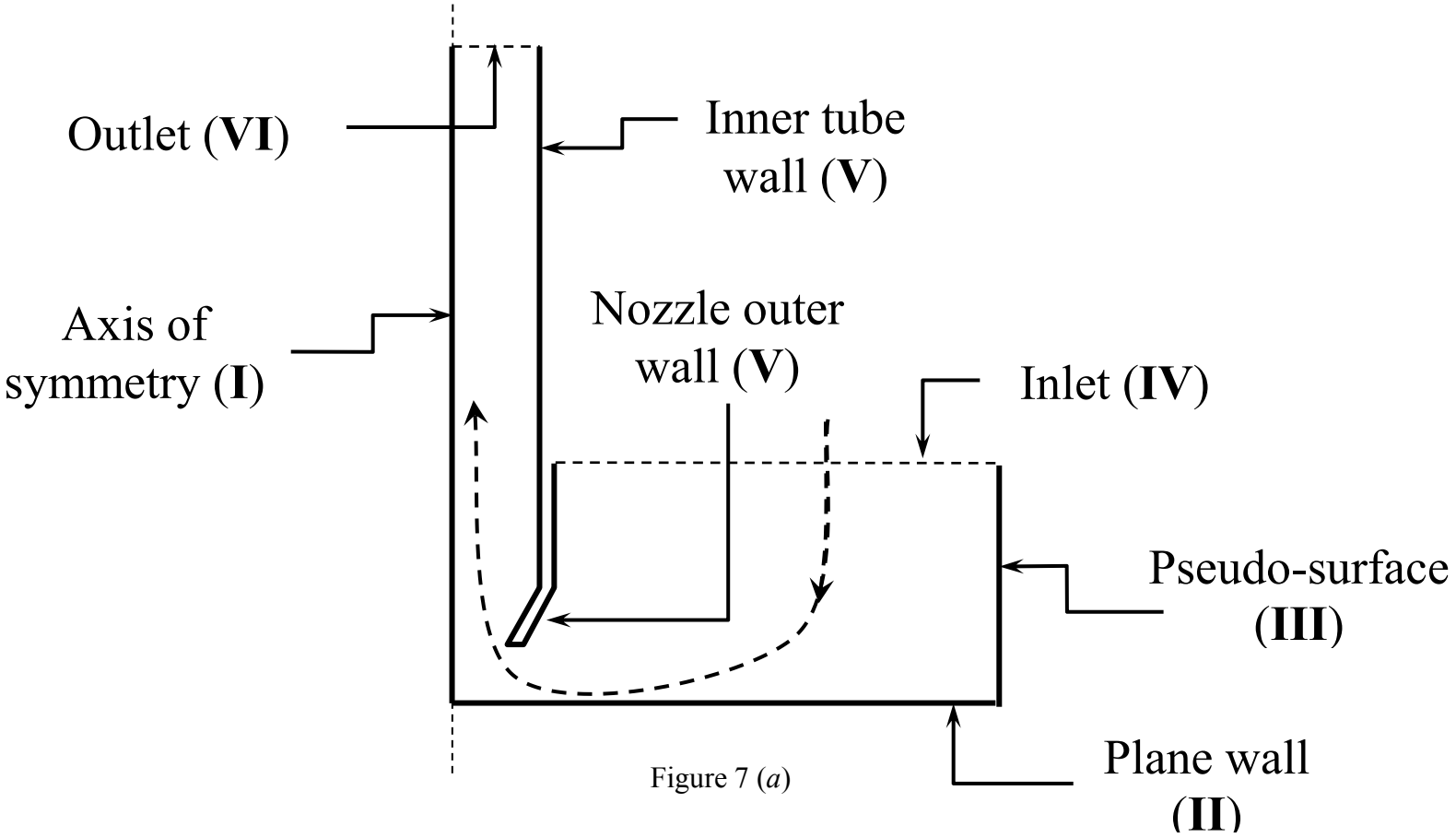

Figure 7 (*a*)

Figure 7: Computational models for different inlet boundary conditions. Boundary tags **I** to **VI** are shown in brackets. (*a*) – Model 1, (*b*) – Model 2, (*c*) – Model 3.

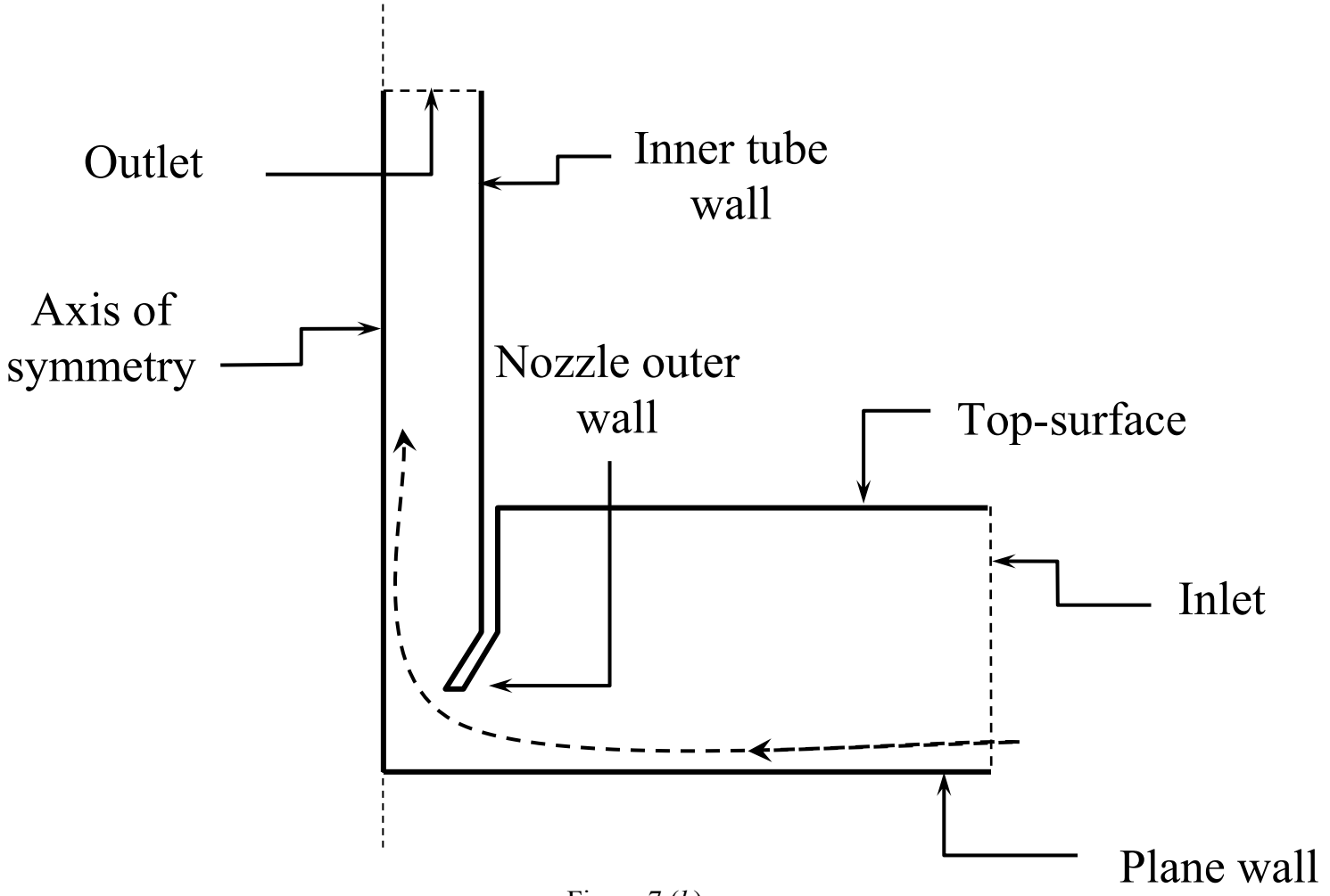
Outlet
Inner tube wall
Axis of symmetry
Nozzle outer wall
Top-surface
Inlet
Plane wall

Figure 7 (*b*)

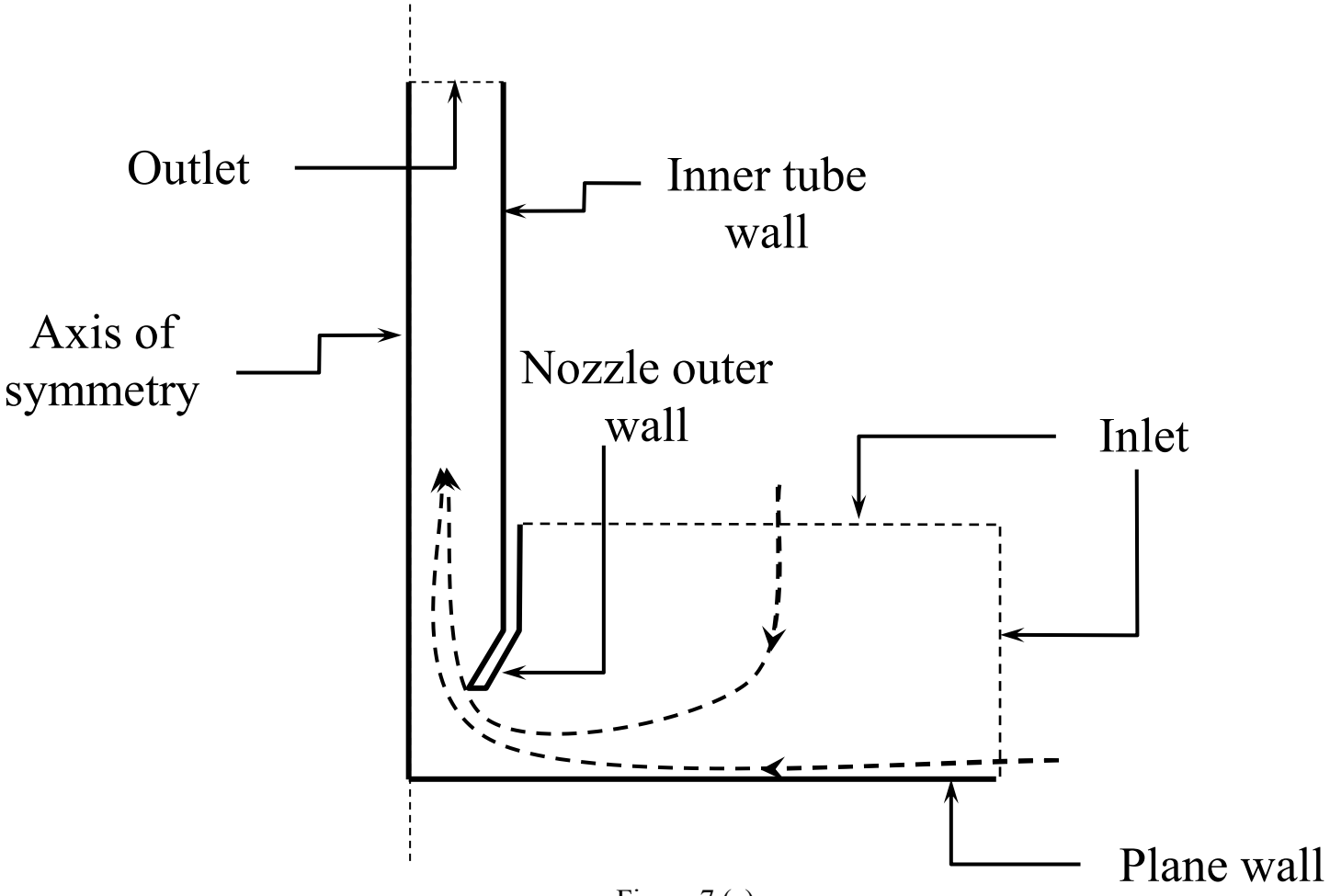
Outlet
Inner tube wall
Axis of symmetry
Nozzle outer wall
Inlet
Plane wall

Figure 7 (*c*)

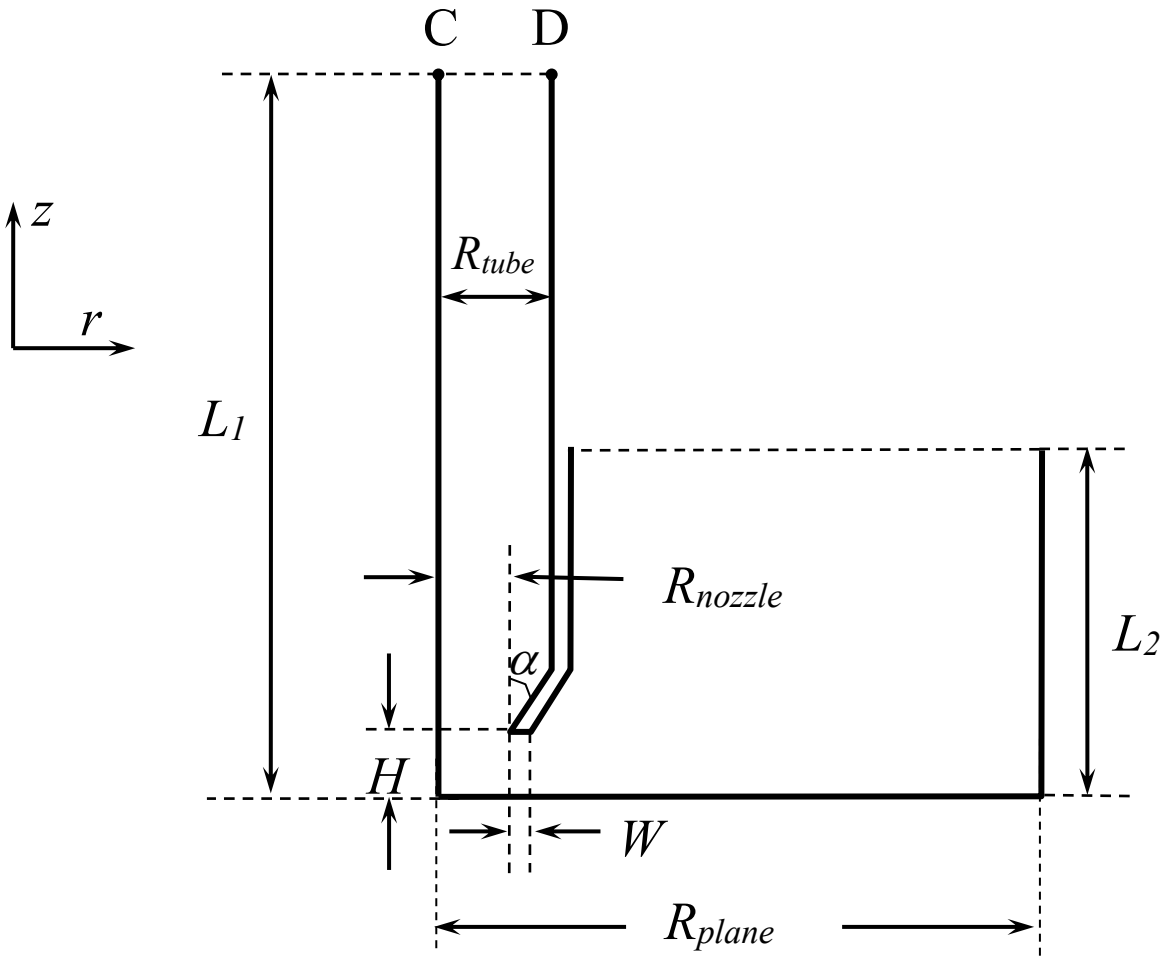

Figure 8: Dimensionless coordinates of the gauging nozzle (R_{tube} = 1).

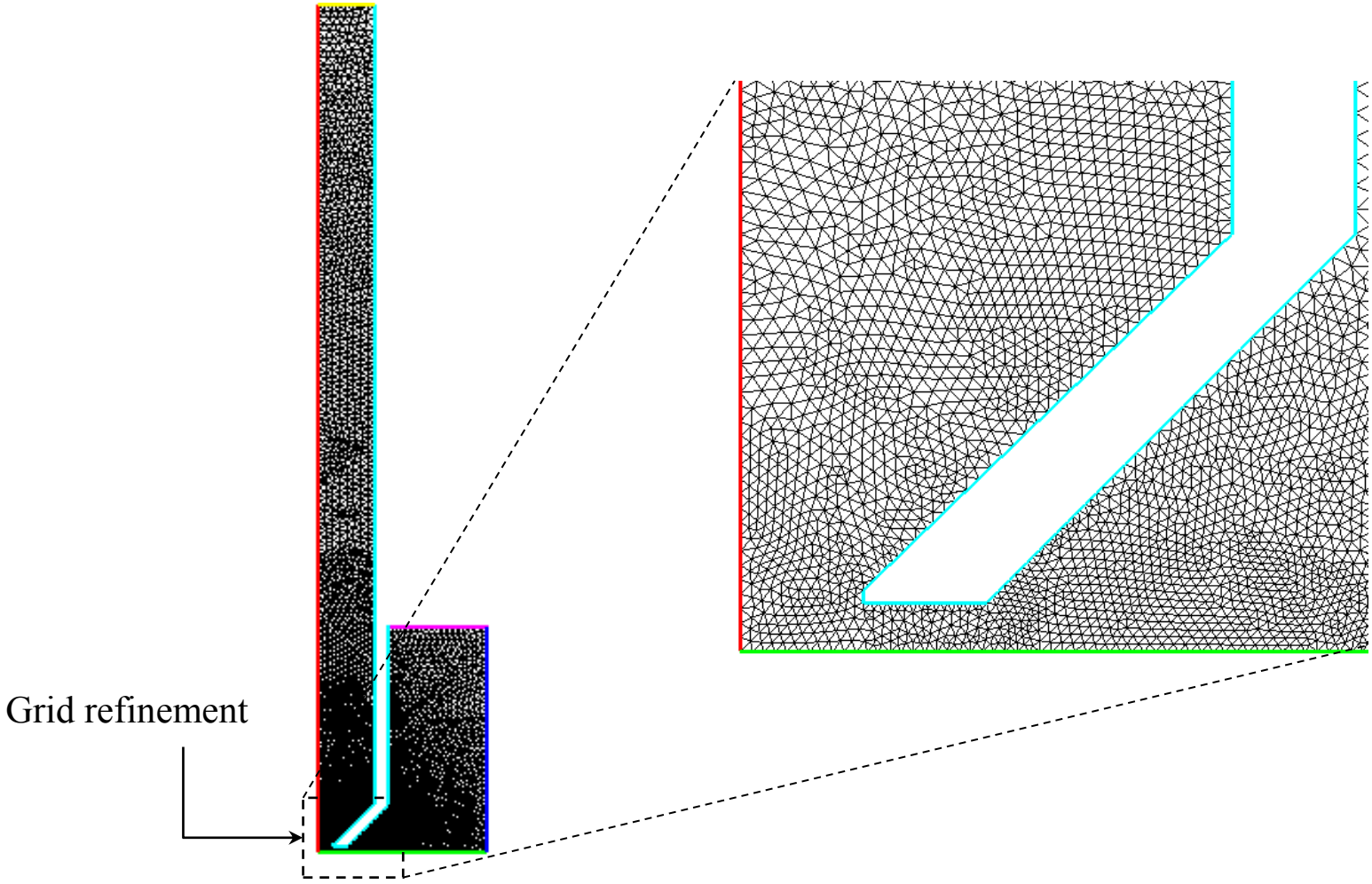

Figure 9: Grid refinement in the region near the nozzle for a typical simulation case.

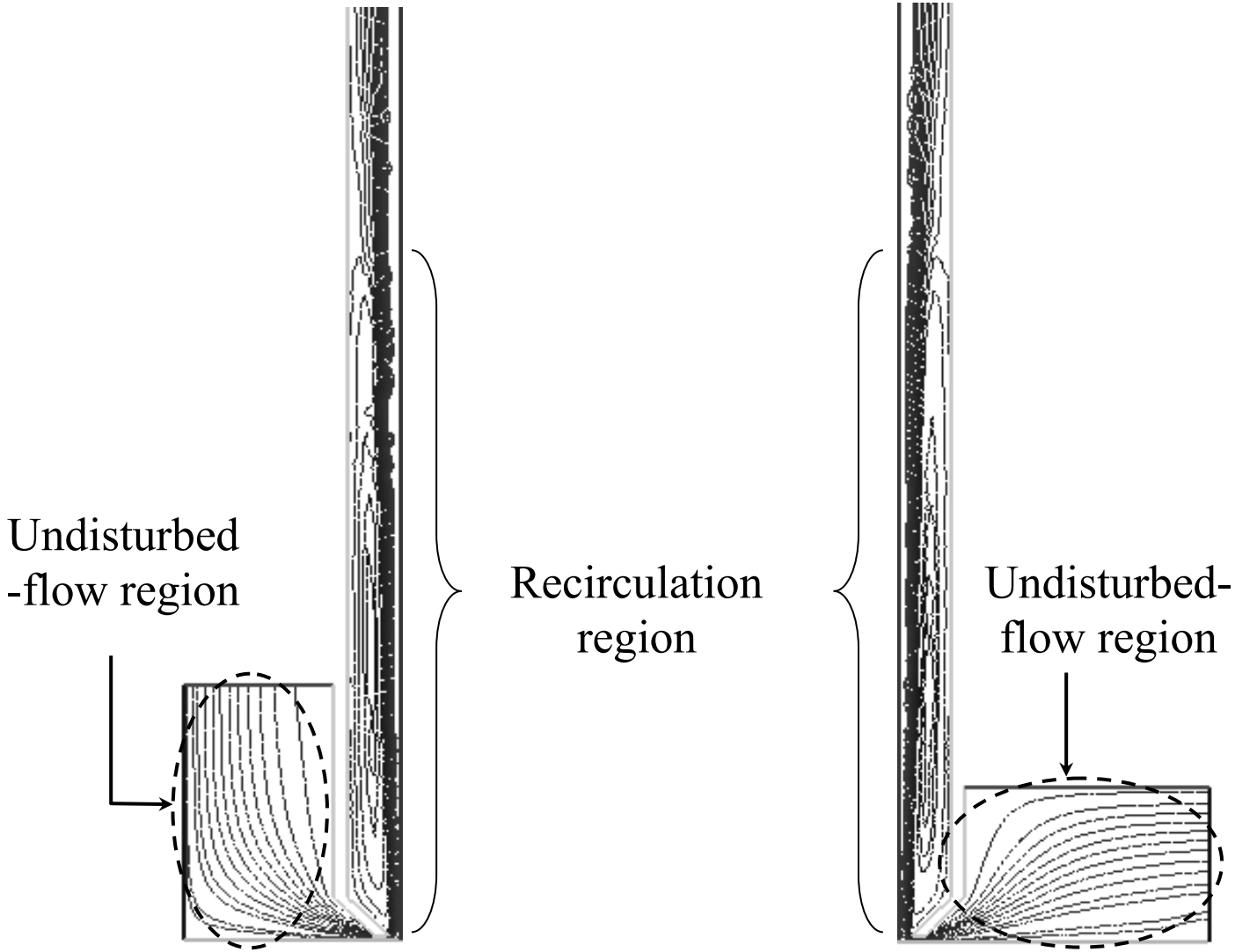

10 (*a*): Model 1

10 (*b*): Model 2

Figure 10: Streamlines at $Re_t = 260$ and $h/d_t = 0.125$ showing three distinct flow regions. (*a*) – Model 1, (*b*) – Model 2, (*c*) – Model 3, (*d*) – Suction region.

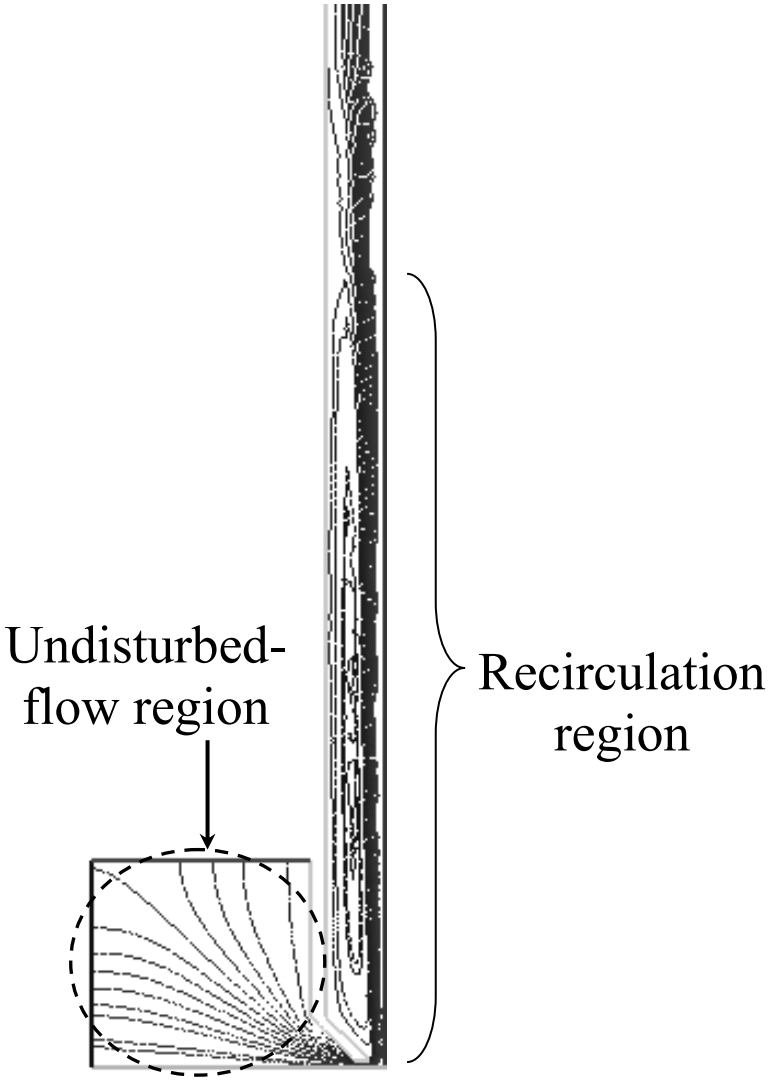

10 (*c*): Model 3

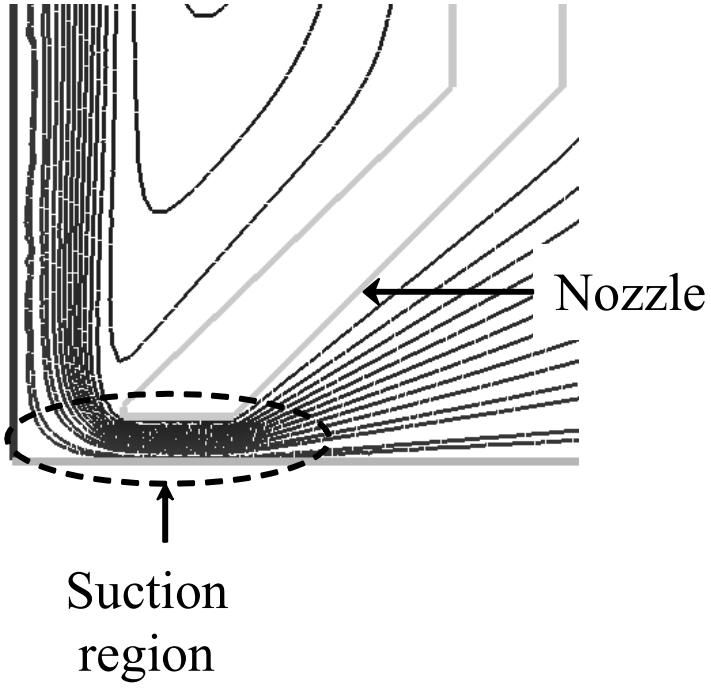

Figure 10 (*d*): Suction region

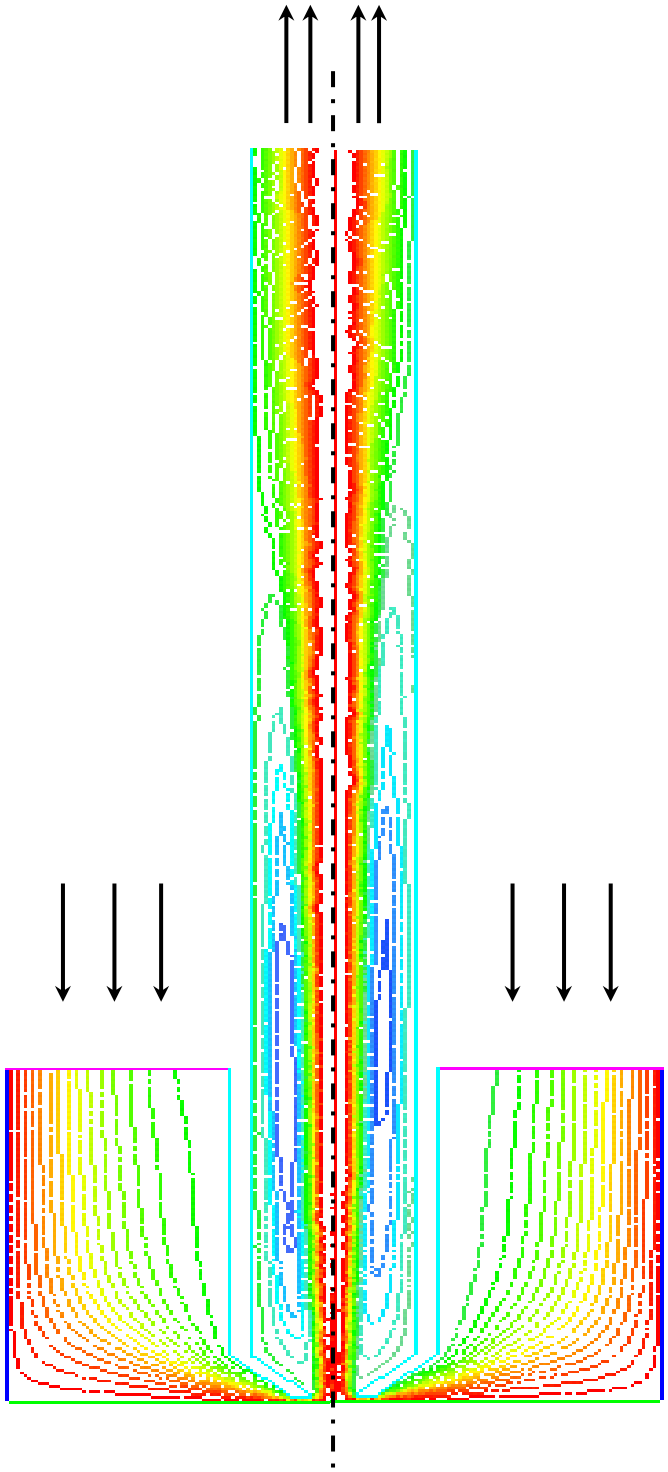

Figure 11(*a*): Streamlines from Model 1 at $h/d_t = 0.2$ and $Re_t = 160$ (left) and 200 (right).

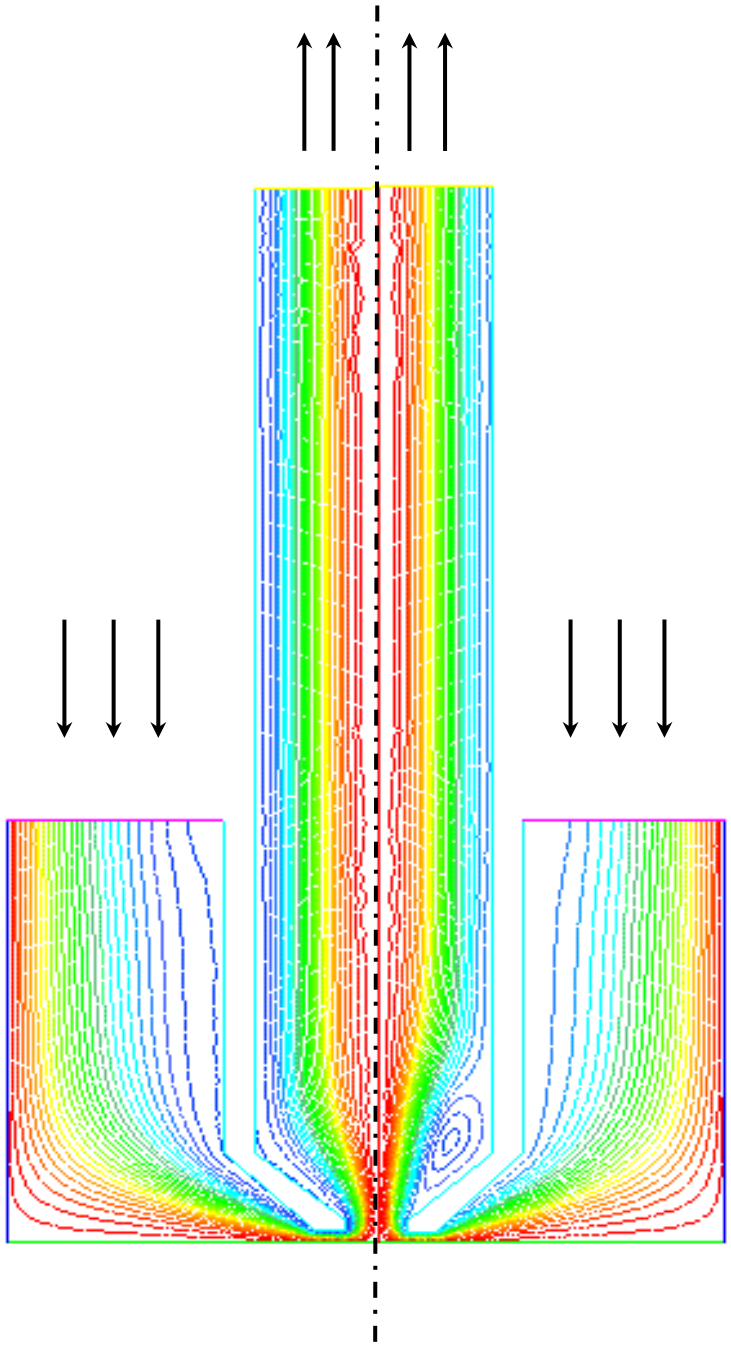

Figure 11(*b*): Streamlines from Model 1 at $h/d_t = 0.2$ and $Re_t = 8$ (left) and 20 (right).

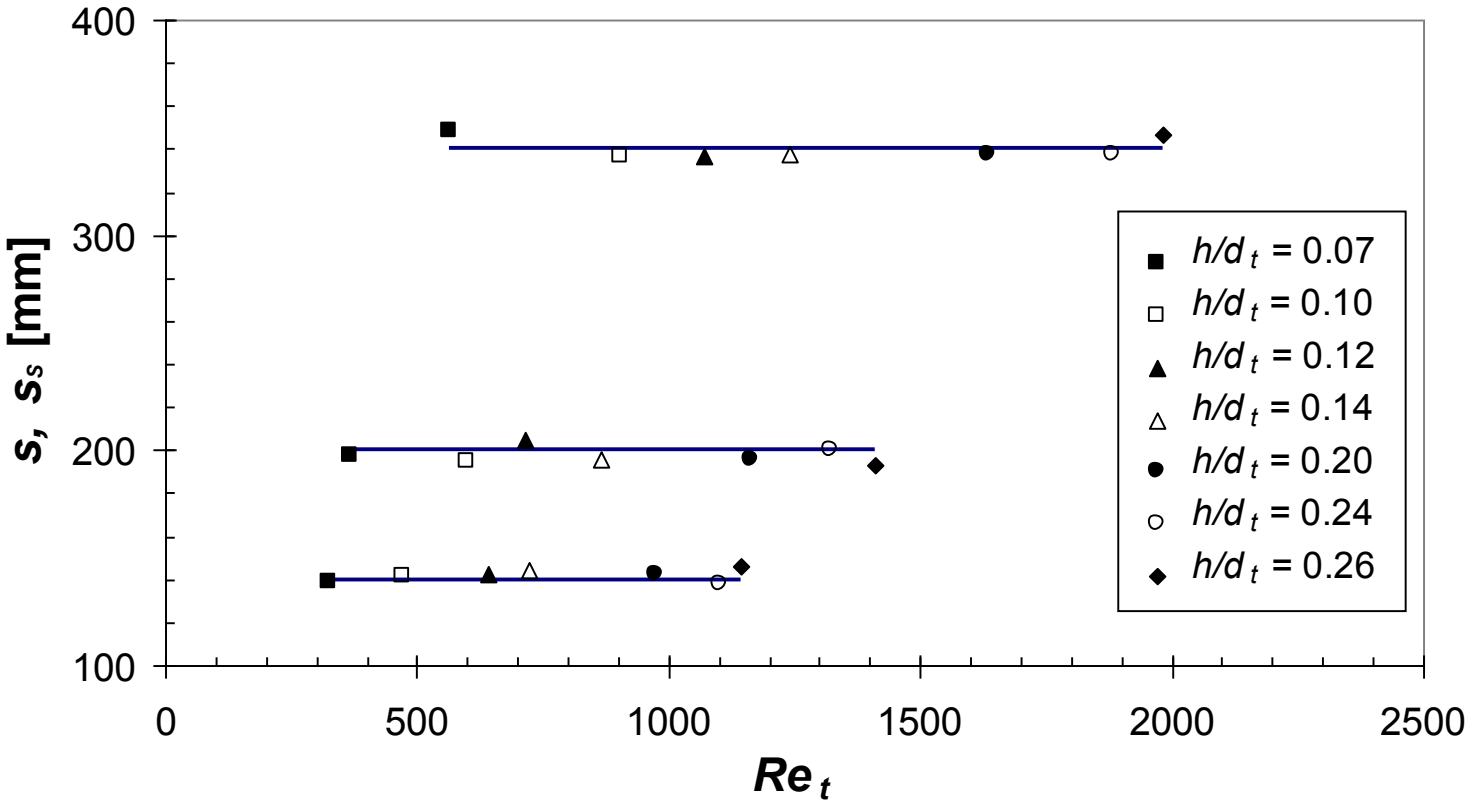

Figure 12: Comparison of hydrostatic head for gauging flows (water).
Symbols - simulation s_s; solid line - experimental s.

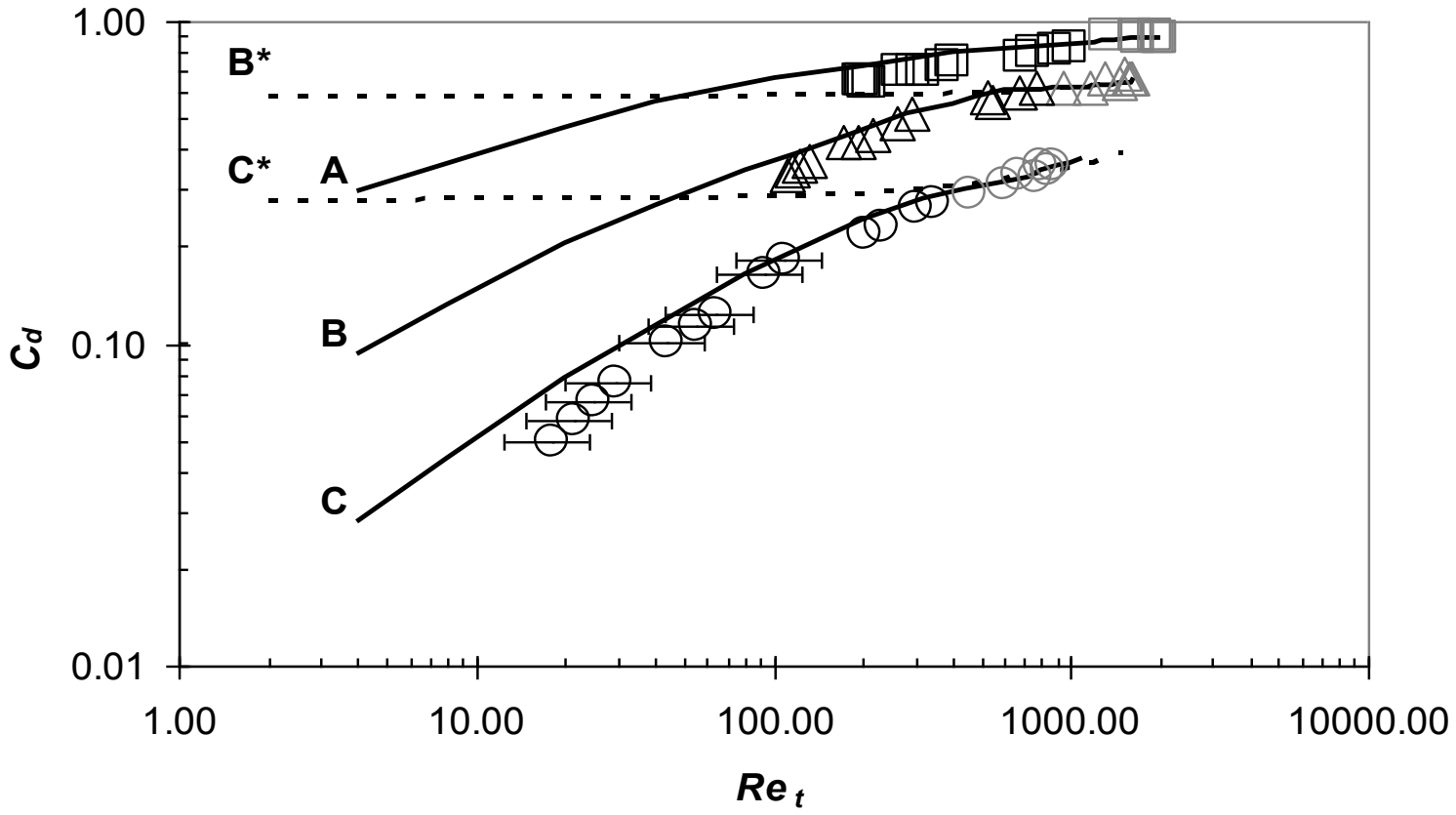

Figure 13(*a*): Discharge coefficient versus Re_t.
Solid lines – this work; **A** – $h/d_t = 0.65$, **B** – $h/d_t = 0.20$, **C** – $h/d_t = 0.10$; symbols – experimental data, black – this work, grey – (Tuladhar, 2001); squares – $h/d_t = 0.65$, triangles – $h/d_t = 0.20$, circles – $h/d_t = 0.10$; dotted lines – empirical model from Tuladhar et al. (2000) – equation (19); **B*** – $h/d_t = 0.20$, **C*** – $h/d_t = 0.10$.
Nozzle: $d_t = 1$ mm, $d = 4$ mm, $w = 0.5$ mm, $\lambda = 0.1$ mm and $\alpha = 45^o$.

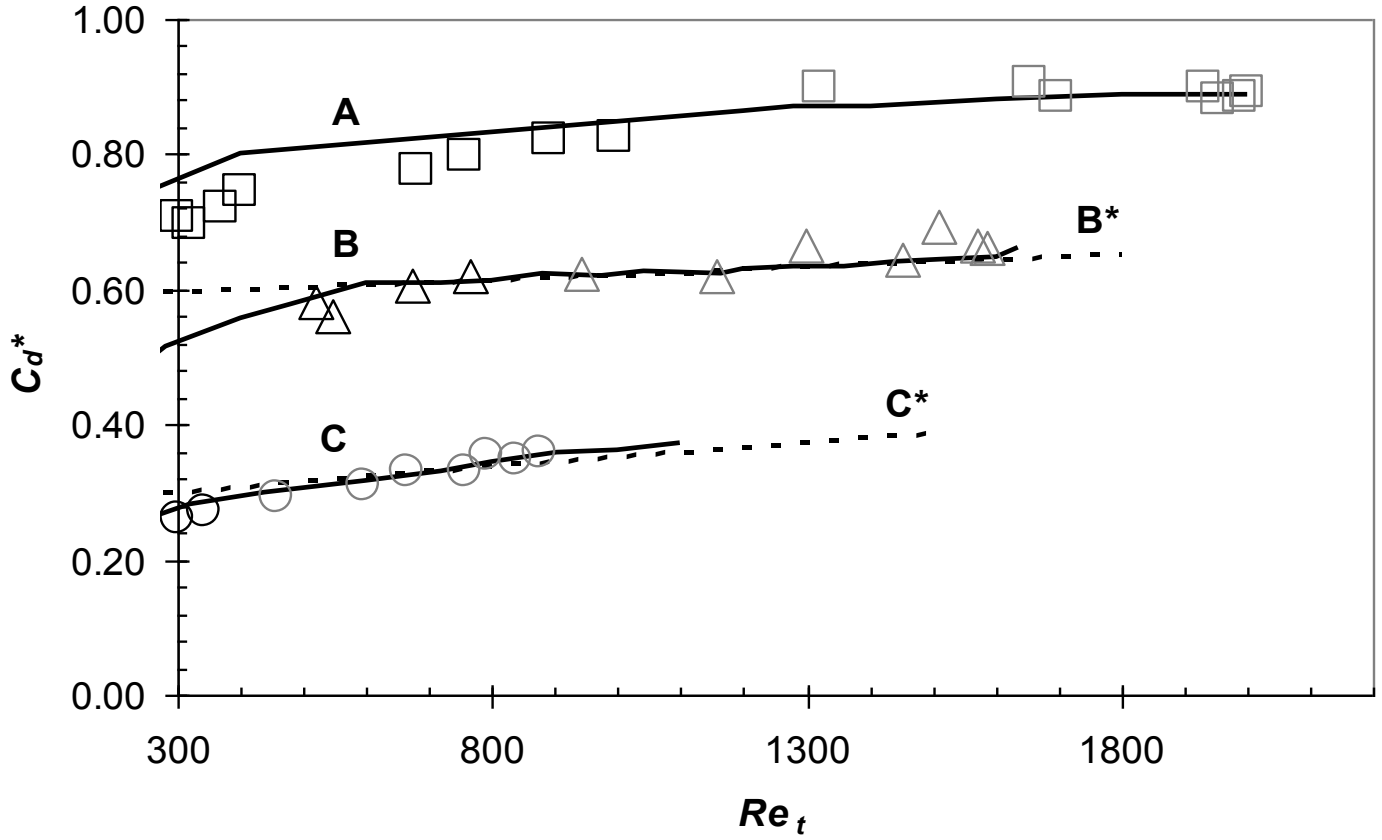

Figure 13(*b*): Asymptotic discharge coefficient versus Re_t, high Re_t range.
Solid lines – this work; **A** – $h/d_t = 0.65$, **B** – $h/d_t = 0.20$, **C** – $h/d_t = 0.10$; symbols – experimental data, black – this work, grey – (Tuladhar, 2001); squares – $h/d_t = 0.65$, triangles – $h/d_t = 0.20$, circles – $h/d_t = 0.10$; dotted lines – empirical model from Tuladhar *et al*. (2000) – equation (19); **B*** – $h/d_t = 0.20$, **C*** – $h/d_t = 0.10$.
Nozzle: $d_t = 1$ mm, $d = 4$ mm, $w = 0.5$ mm, $\lambda = 0.1$ mm and $\alpha = 45^o$.

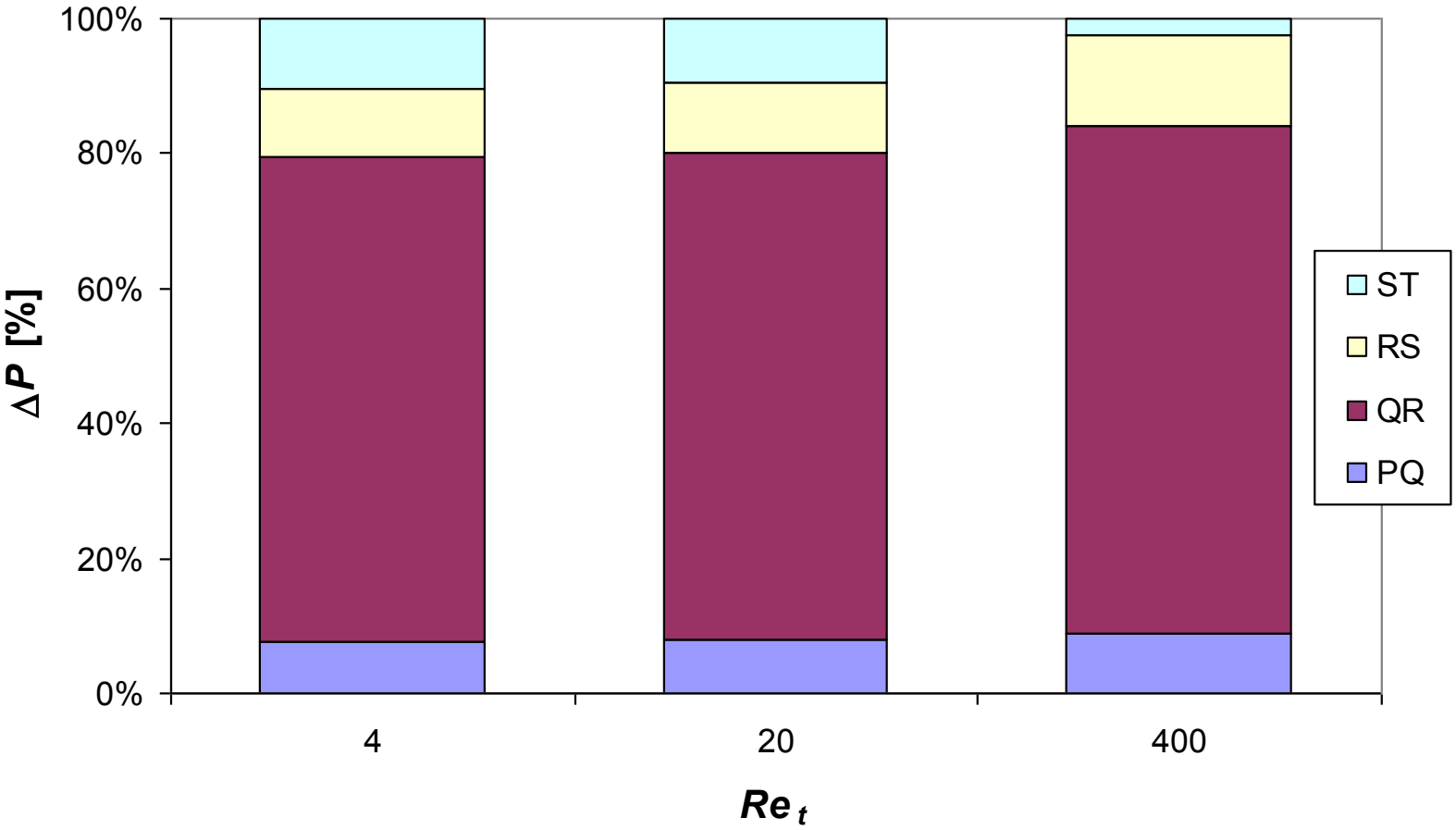

Figure 14 (*a*): Pressure drop analysis, $h/d_t = 0.10$.

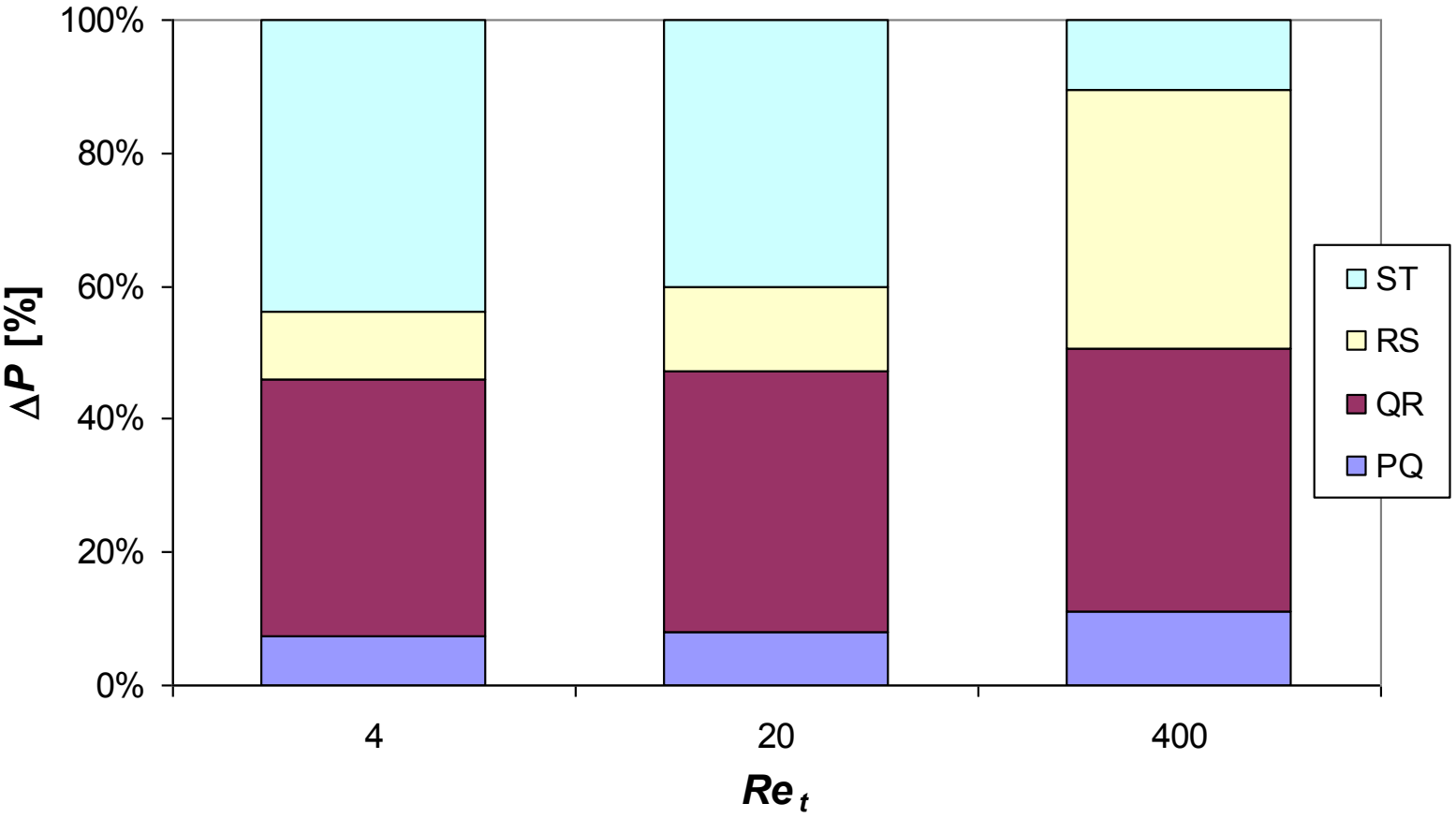

Figure 14 (*b*): Pressure drop analysis, $h/d_t = 0.20$.

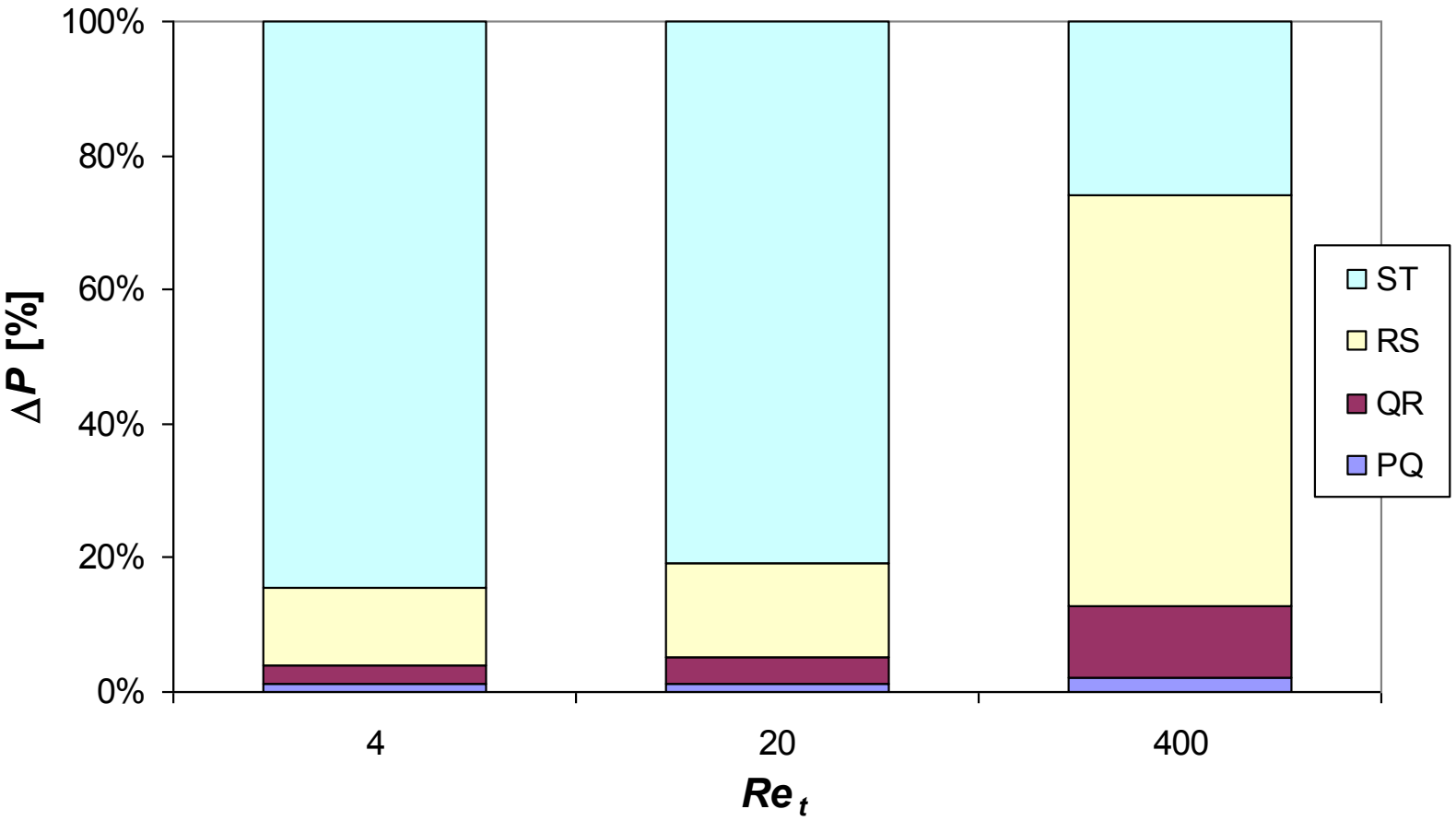

Figure 14 (*c*): Pressure drop analysis, $h/d_t = 0.65$.

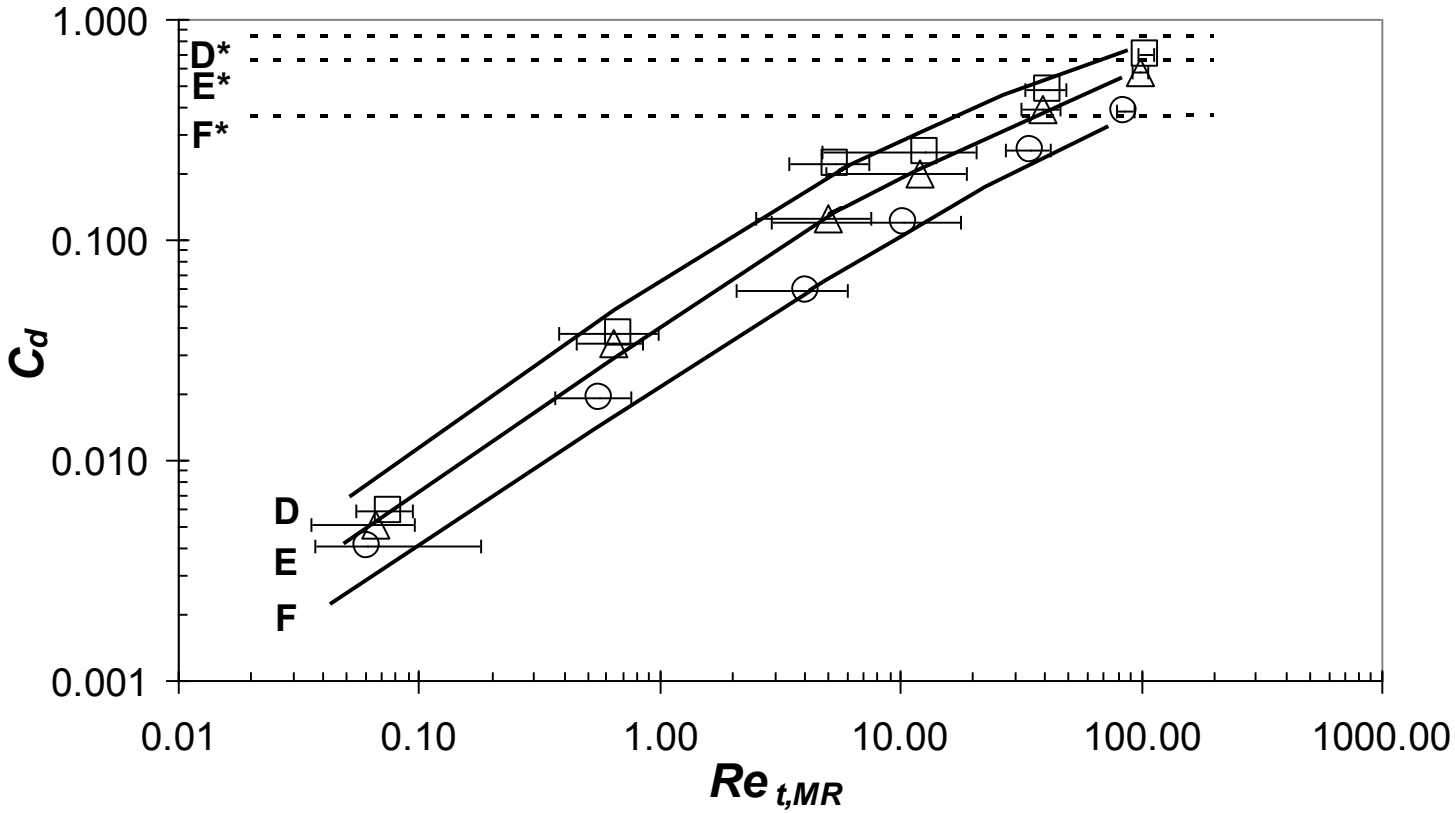

Figure 15: Discharge coefficient versus Re_t for CMC solutions.
Solid lines – this work; **D** – $h/d_t = 0.34$, **E** – $h/d_t = 0.18$, **F** – $h/d_t = 0.10$; symbols – experimental data (Colombo and Steynor, 2002); squares – $h/d_t = 0.34$, triangles – $h/d_t = 0.18$, circles – $h/d_t = 0.10$; dotted lines – empirical model from Tuladhar (2001) – equation (26); **D*** – 0.34, **E*** – $h/d_t = 0.18$, **F*** – $h/d_t = 0.10$.
Nozzle: $d_t = 2$ mm, $d = 4$ mm, $w = 0.2$ mm, $\lambda = 0.1$ mm and $\alpha = 30^o$.

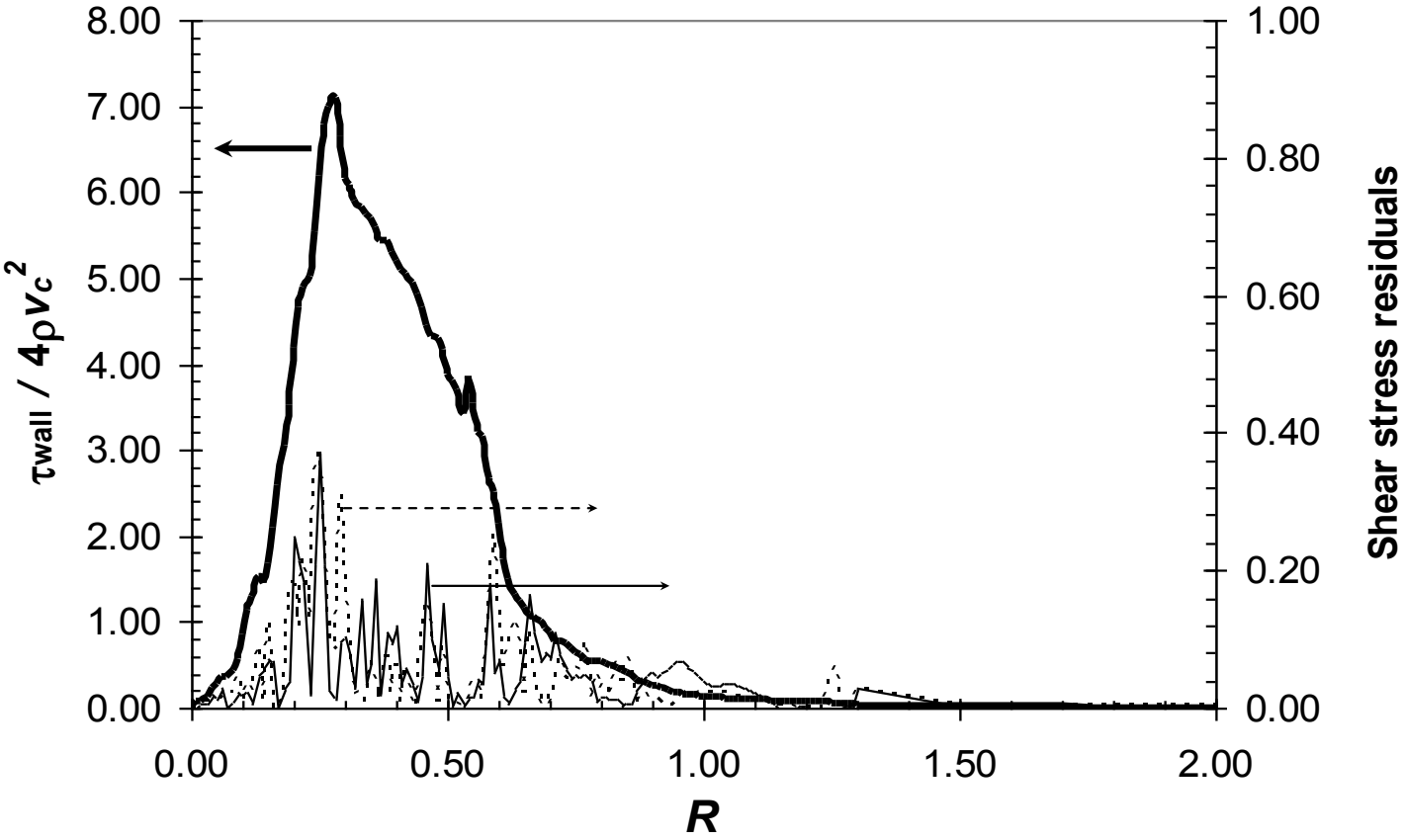

Figure 16(*a*): Dimensionless shear stress distributions on the gauged surface. Case : $Re_t = 260$, $h/d_t = 0.125$.
Thick solid line, Model 1; thin solid line, τ_{wall} residuals (dimensionless) from Model 2 (equation (27)); dotted line, τ_{wall} residuals (dimensionless) from Model 3 (equation (28)).
Nozzle: $d_t = 1.0$ mm, $d = 4.0$ mm, $\lambda = 0.1$ mm and $w = 0.5$ mm.

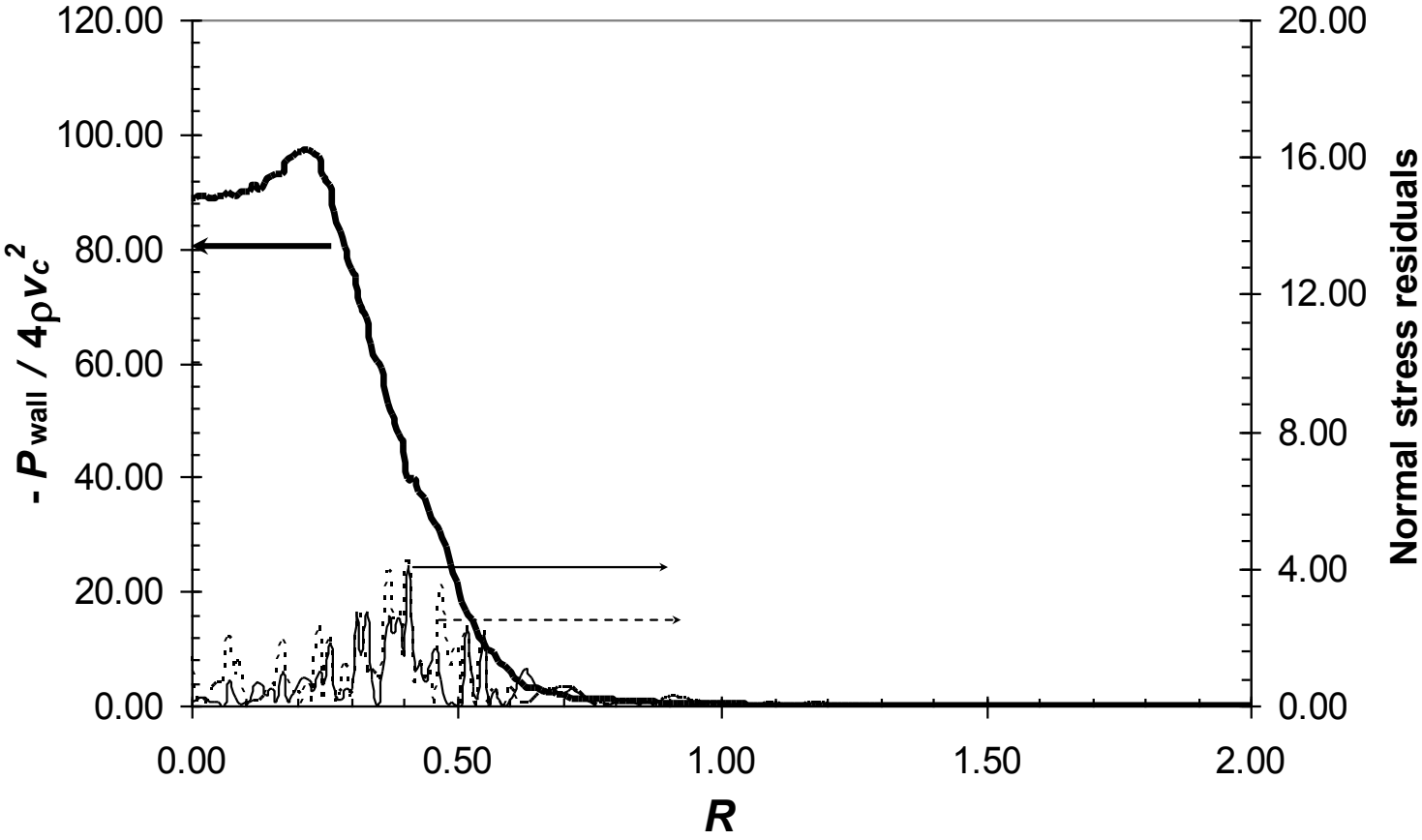

Figure 16(*b*): Dimensionless normal stress distributions on the gauged surface. Case: $Re_t = 260$, $h/d_t = 0.125$.
Thick solid line, Model 1; thin solid line, - P_{wall} residuals (dimensionless) for Model 2 (equation (27)); dotted line, -P_{wall} residuals (dimensionless) for Model 3 (equation (28)).
Nozzle: $d_t = 1.0$ mm, $d = 4.0$ mm, $\lambda = 0.1$ mm and $w = 0.5$ mm.

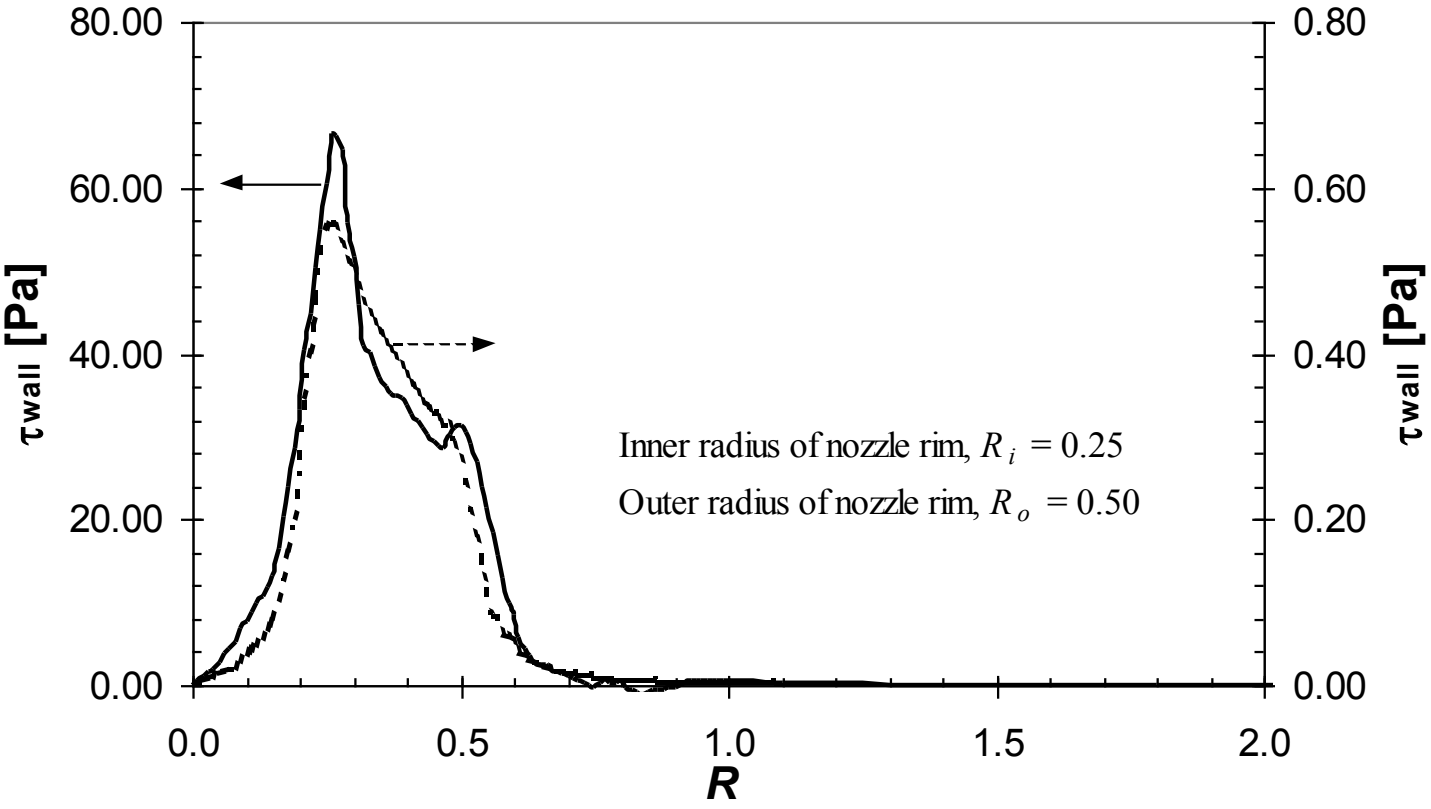

Figure 17(*a*): Shear stress distributions on the gauged surface, Case: $h/d_t = 0.10$. Solid line, $Re_t = 904$; dotted line, $Re_t = 4$.

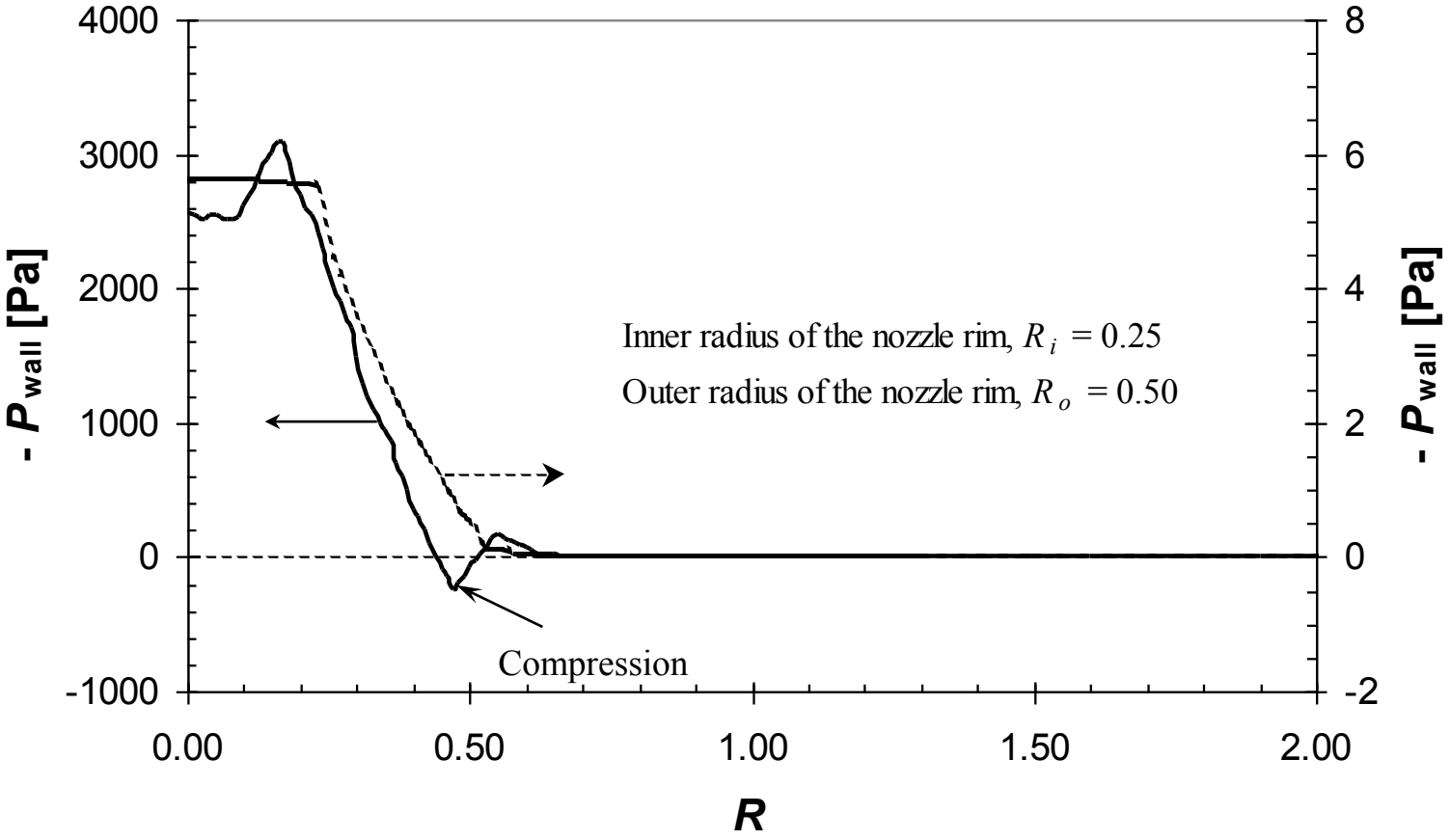

Figure 17(*b*): Normal stress distributions on the gauged surface, Case: $h/d_t = 0.10$. Solid line, $Re_t = 904$; dotted line, $Re_t = 4$.

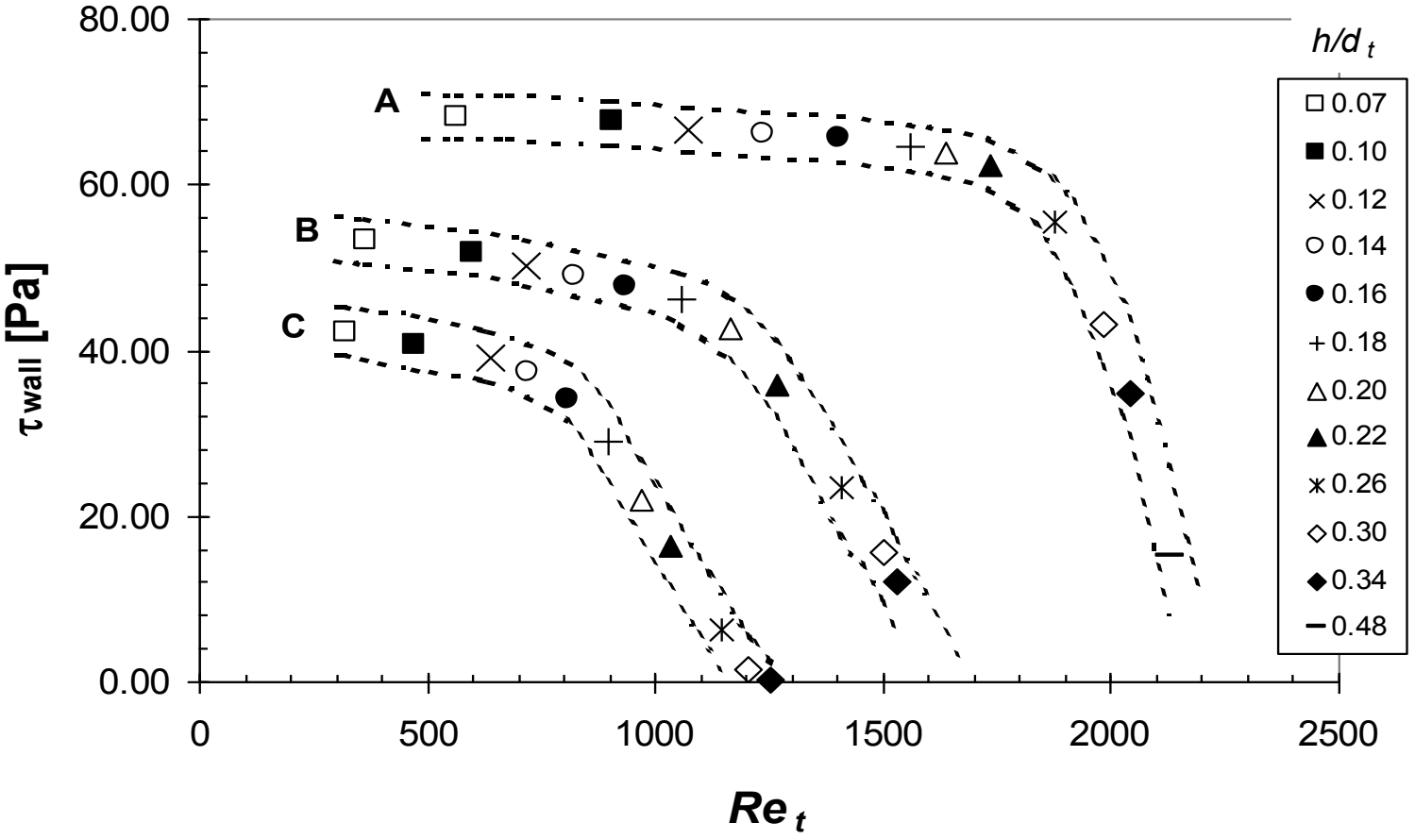

Figure 18: Maximum wall shear stress versus Re_t (water).
Identification of data sets: **A** - s = 340 mm; **B** – s = 200 mm; **C** – s = 140 mm.

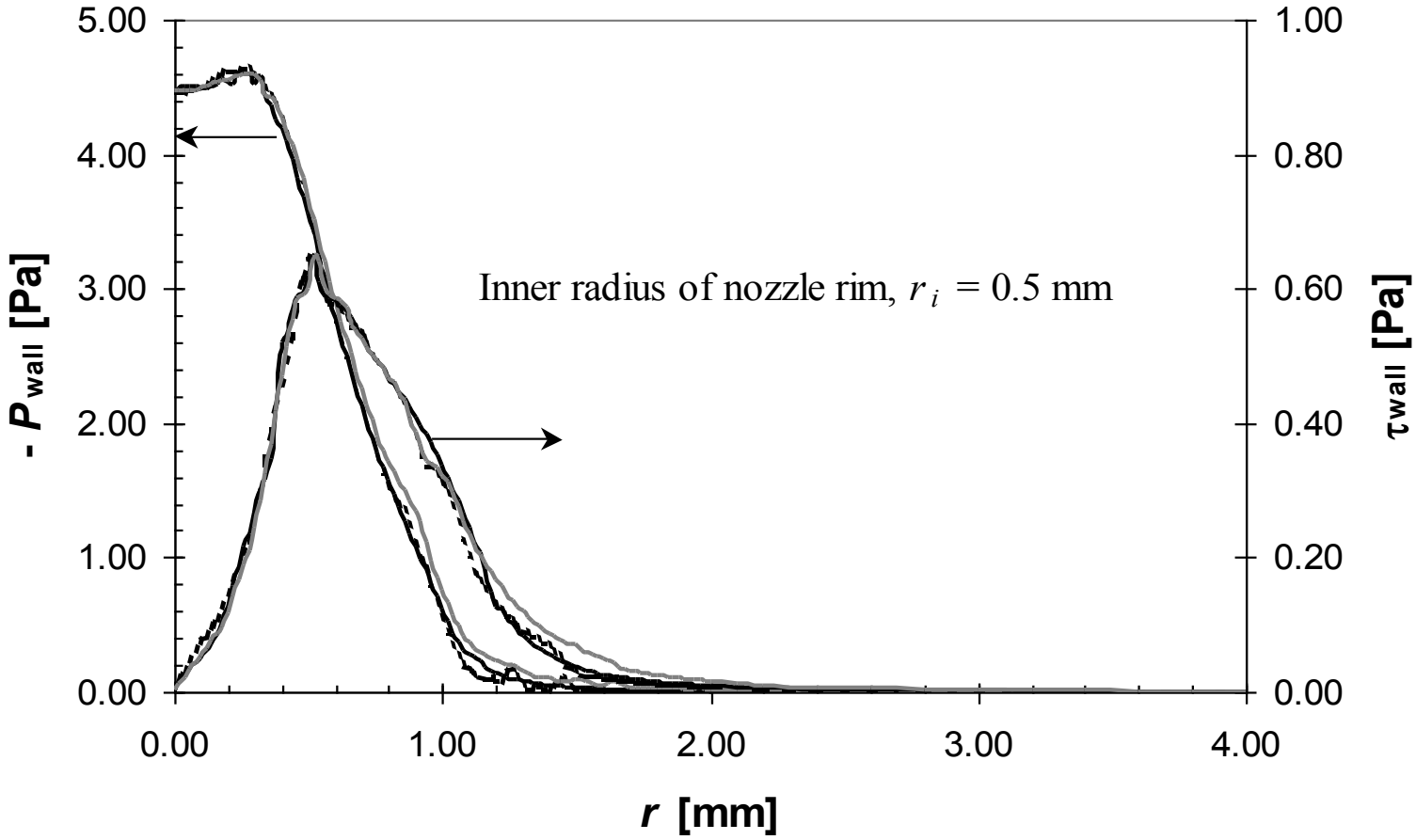

Figure 19(*a*): Shear and normal stress distributions on the gauged surface, Case: $Re_t = 20$, $h/d_t = 0.20$.
Nozzle: $d_t = 1.0$ mm, $d = 4.0$ mm, $\lambda = 0.1$ mm and $w = 0.5$ mm.
Grey solid line, $\alpha = 60^o$, black solid line, $\alpha = 45^o$, dotted line, $\alpha = 30^o$.

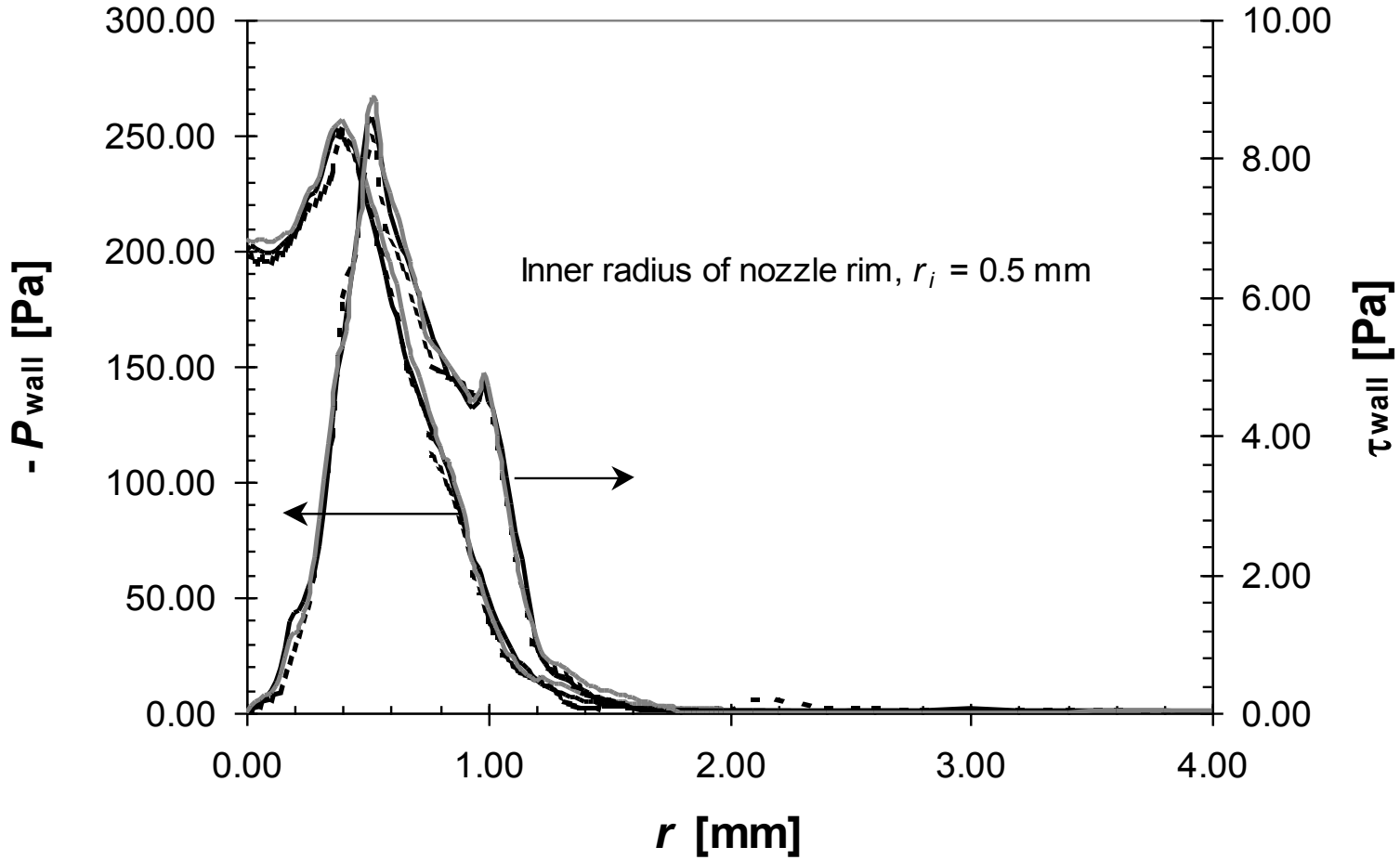

Figure 19(*b*): Shear and normal stress distributions on the gauged surface, Case: $Re_t = 400$, $h/d_t = 0.20$.
Nozzle: $d_t = 1.0$ mm, $d = 4.0$ mm, $\lambda = 0.1$ mm and $w = 0.5$ mm.
Grey solid line, $\alpha = 60^o$, black solid line, $\alpha = 45^o$, dotted line, $\alpha = 30^o$.

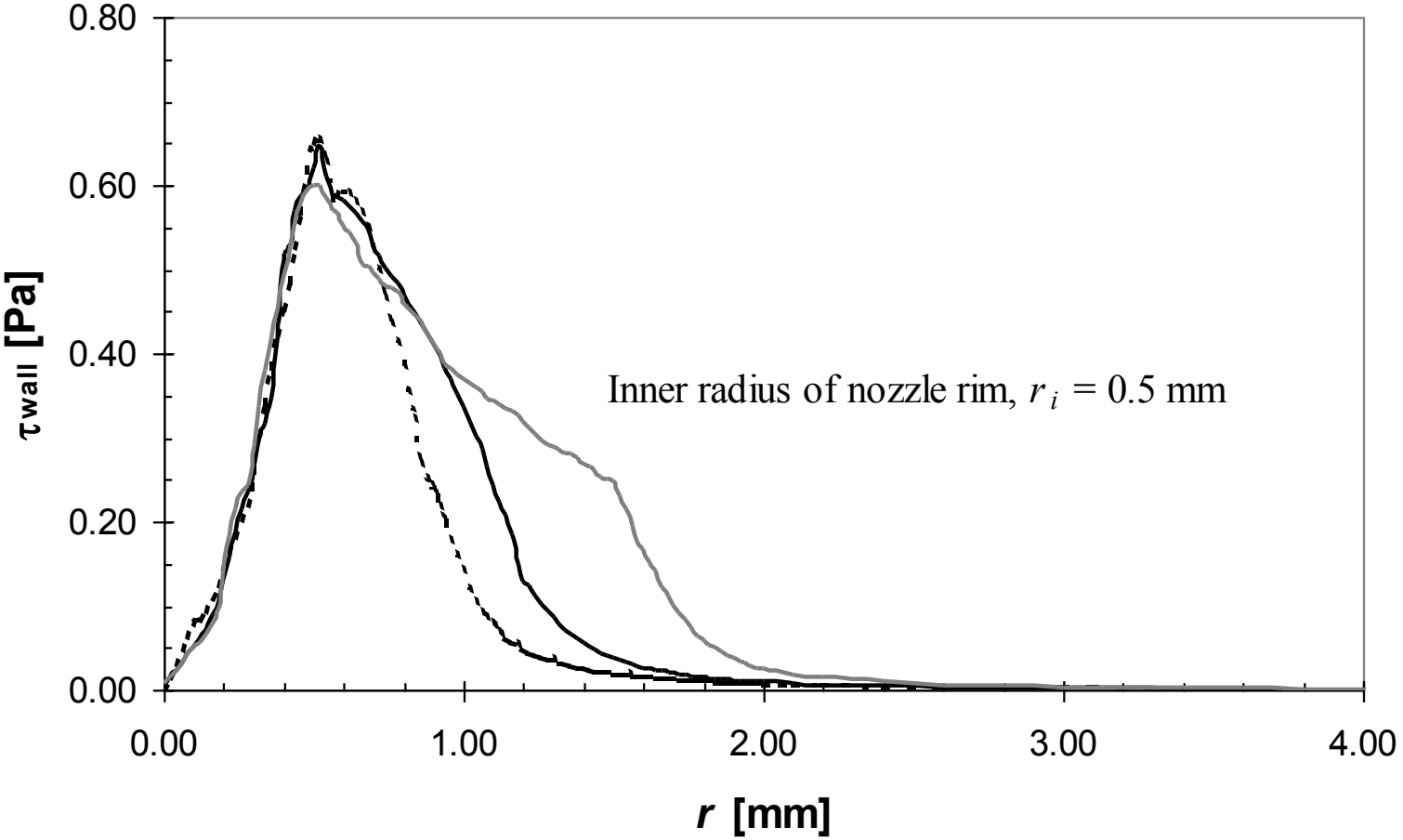

Figure 20(*a*): Shear stress distributions on the gauged surface, Case: $Re_t = 20$, $h/d_t = 0.20$.
Nozzle: $d_t = 1.0$ mm, $d = 4.0$ mm, $\lambda = 0.1$ mm and $\alpha = 45^o$.
Grey solid line, $w = 1.0$ mm, black solid line, $w = 0.5$ mm, dotted line, $w = 0.25$ mm.

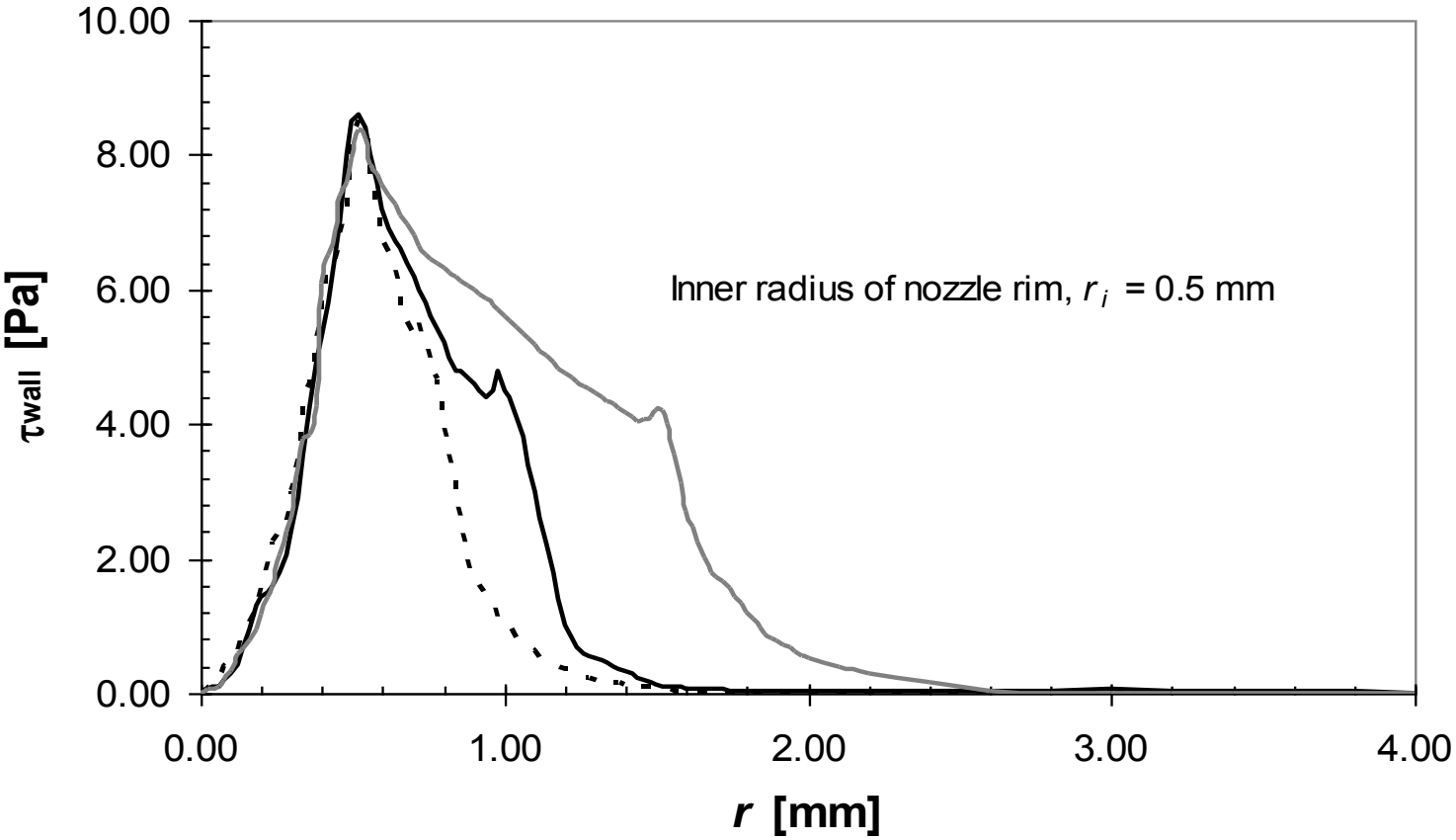

Figure 20(*b*): Shear stress distributions on the gauged surface, Case: $Re_t = 400$, $h/d_t = 0.20$.
Nozzle: $d_t = 1.0$ mm, $d = 4.0$ mm, $\lambda = 0.1$ mm and $\alpha = 45^o$.
Grey solid line, $w = 1.0$ mm, black solid line, $w = 0.5$ mm, dotted line, $w = 0.25$ mm.

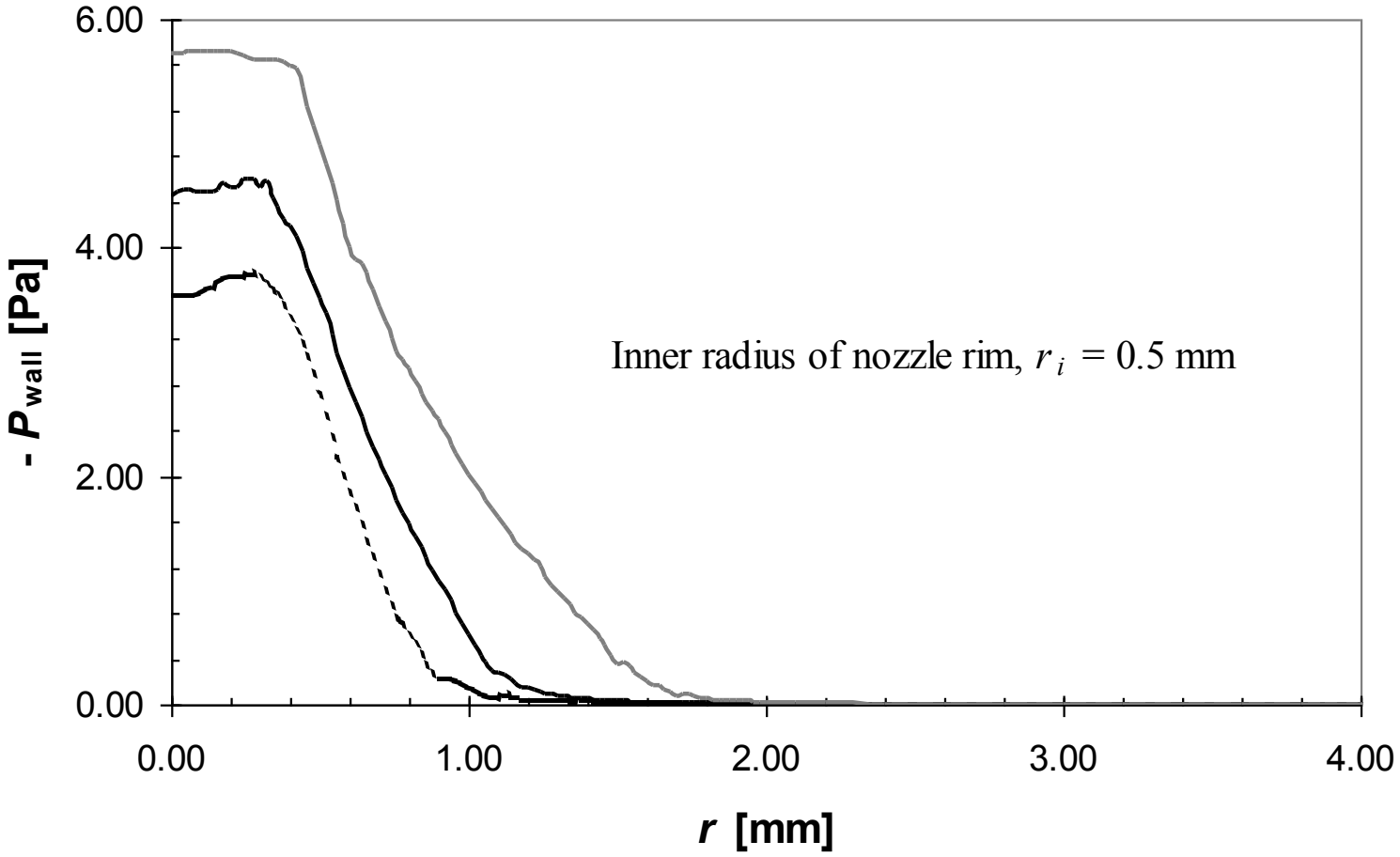

Figure 20(*c*): Normal stress distributions on the gauged surface, Case: $Re_t = 20$, $h/d_t = 0.20$.
Nozzle: $d_t = 1.0$ mm, $d = 4.0$ mm, $\lambda = 0.1$ mm and $\alpha = 45^o$.
Grey solid line, $w = 1.0$ mm, black solid line, $w = 0.5$ mm, dotted line, $w = 0.25$ mm.

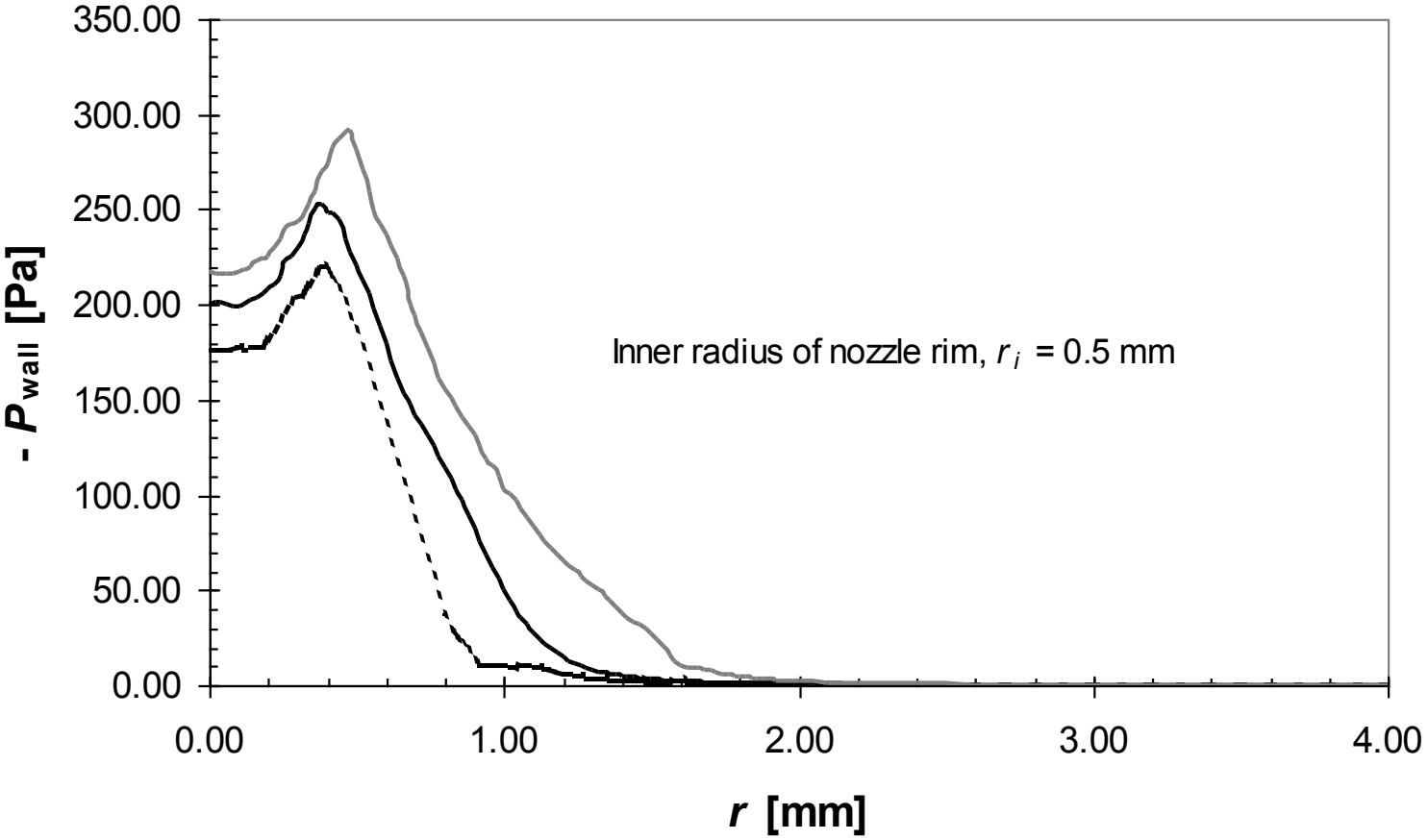

Figure 20 (*d*): Normal stress distributions on the gauged surface, Case: $Re_t = 400$, $h/d_t = 0.20$.
Nozzle: $d_t = 1.0$ mm, $d = 4.0$ mm, $\lambda = 0.1$ mm and $\alpha = 45^o$.
Grey solid line, $w = 1.0$ mm, black solid line – $w = 0.5$ mm, dotted line – $w = 0.25$ mm.

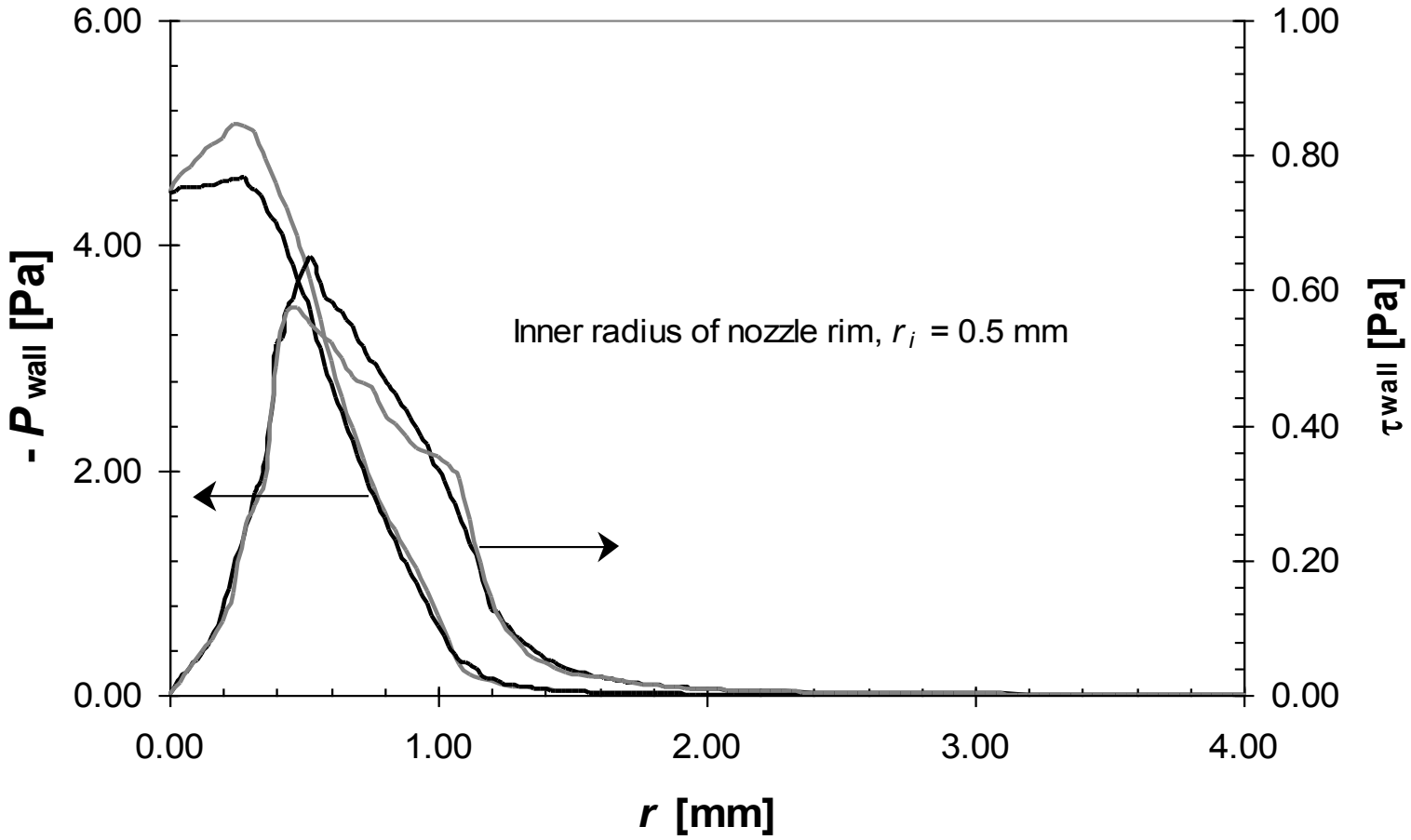

Figure 21 (*a*): Shear stress distributions on the gauged surface, Case: $Re_t = 20$, $h/d_t = 0.20$.
Nozzle: $d_t = 1.0$ mm, $w = 0.5$ mm, $\lambda = 0.1$ mm and $\alpha = 45^o$.
Grey solid line, $d = 8.0$ mm, black solid line, $d = 4.0$ mm.

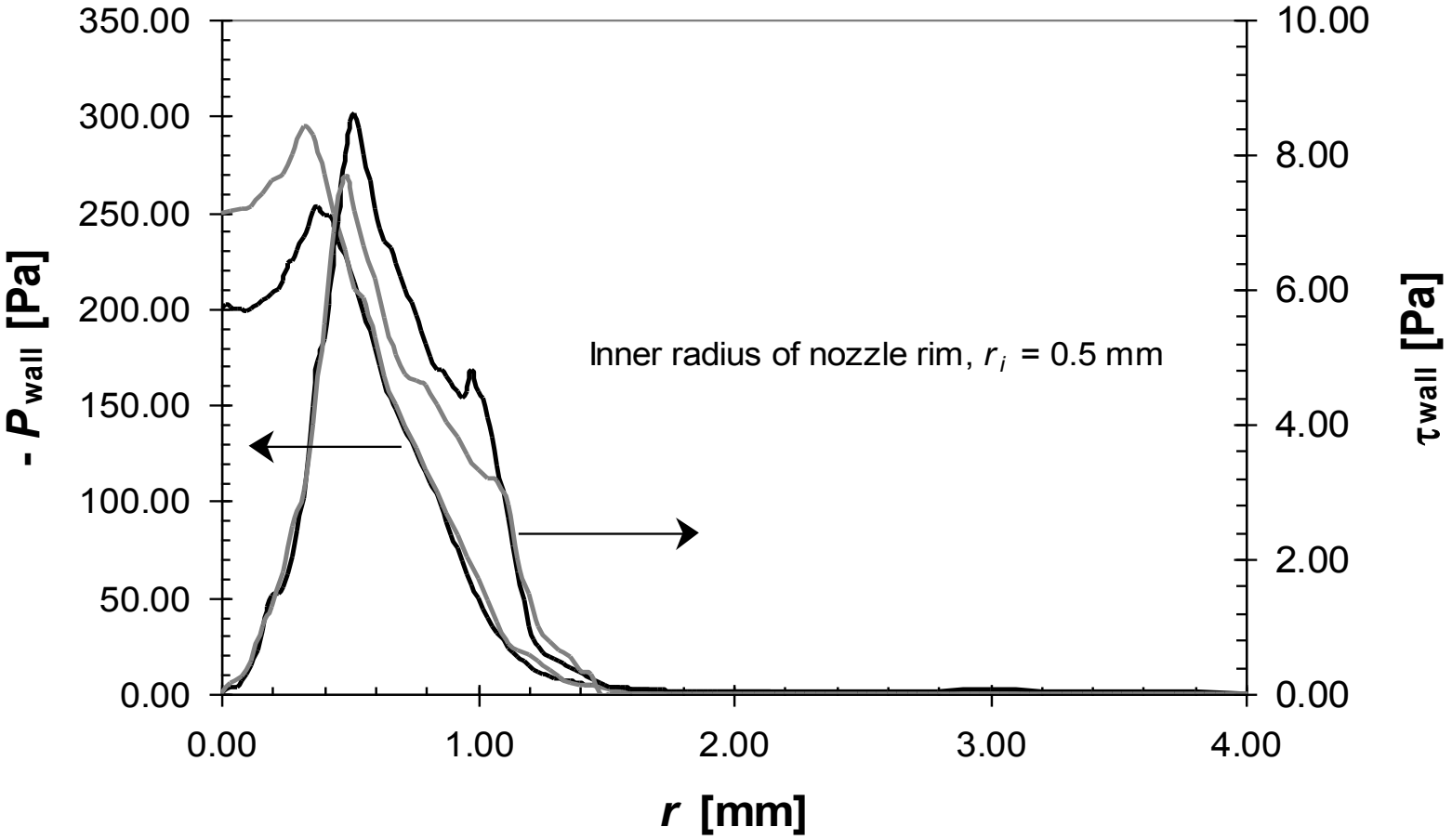

Figure 21 (*b*): Shear stress distributions on the gauged surface, Case: $Re_t = 400$, $h/d_t = 0.20$.
Nozzle: $d_t = 1.0$ mm, $w = 0.5$ mm, $\lambda = 0.1$ mm and $\alpha = 45^o$.
Grey solid line, $d = 8.0$ mm, black solid line, $d = 4.0$ mm.

	$0 \leq \boldsymbol{Re_t} \leq 200$	$201 \leq \boldsymbol{Re_t} \leq 1000$	$1001 \leq \boldsymbol{Re_t} \leq 1500$	$1501 \leq \boldsymbol{Re_t} \leq 2200$
$0.07 \leq \boldsymbol{h/d_t} \leq 0.10$	$30 \times R_{tube}$	$90 \times R_{tube}$	–	–
$0.11 \leq \boldsymbol{h/d_t} \leq 0.20$	$30 \times R_{tube}$	$100 \times R_{tube}$	$130 \times R_{tube}$	–
$0.21 \leq \boldsymbol{h/d_t} \leq 0.30$	$30 \times R_{tube}$	$90 \times R_{tube}$	$110 \times R_{tube}$	$130 \times R_{tube}$
$0.31 \leq \boldsymbol{h/d_t} \leq 0.50$	$20 \times R_{tube}$	$70 \times R_{tube}$	$100 \times R_{tube}$	$110 \times R_{tube}$
$0.51 \leq \boldsymbol{h/d_t} \leq 0.65$	$20 \times R_{tube}$	$70 \times R_{tube}$	$100 \times R_{tube}$	$110 \times R_{tube}$

Table 1: Summary of the values of L_1 used in the simulations.

Sucrose solution (w/w %)	Viscosity (kg/ms)	
	Experimental	Mathlouthi and Genotelle (1995)
15%	0.00145	0.00140
25%	0.00224	0.00215
35%	0.00373	0.00374

Table 2: Summary of the viscosities for sucrose solutions at 25^{o}C.

- 0.34

CMC solution (w/w %)	*n*	*k*
0.8% high viscosity	0.59	0.60
0.5% high viscosity	0.61	0.40
0.3% high viscosity	0.67	0.18
0.8% low viscosity	0.85	0.033
0.5% low viscosity	0.93	0.0106
0.3% low viscosity	0.98	0.0044

Table 3: Summary of the rheological parameters for CMC solution at 25°C (Colombo & Steynor, 2002).